DETERMINING EFFECTIVE LIFETIME OF MINORITY CARRIERS IN SILICON THROUGH MODULATED FREE CARRIER ABSORPTION

DETERMINING EFFECTIVE LIFETIME OF MINORITY CARRIERS IN SILICON THROUGH MODULATED FREE CARRIER ABSORPTION

By KARL PETURSSON, B.Sc.

A Thesis Submitted to the School of Graduate Studies in Partial Fulfillment of the Requirements for the Degree of Master of Applied Science

Master of Applied Science (2017) McMaster University
Engineering Physics Hamilton, Ontario, Canada

Title: Determining Effective Lifetime of Minority Carriers in Silicon Through Modulated Free Carrier Absorption

Author: Karl Petursson, B.Sc (Physics and Astronomy Specialist)

Supervisor: Dr. Rafael Kleiman

Pages: Viii, 74

Abstract

The minority carrier lifetime is a valuable parameter for determining the electrical properties of semiconductors. It is particularly useful in the fabrication of solar cells as minority carrier lifetime is directly related to device efficiency. Pump-probe techniques, in which a pump laser of photon energy above the bandgap energy of the material is used to excite free carrier populations while a sub-bandgap probe laser is used to monitor the change in excess carrier density have been demonstrated to be an effective, non-contact, method to measure the minority carrier lifetime, particularly well-suited for use as an in-line measurement apparatus for the solar cell manufacturing processes

In this thesis a non-contact, optical, pump-probe method has been used to determine the minority carrier lifetime of float zone and Czochralski grown <100> silicon samples through measurements of modulated free carrier absorption. The equivalence between measurements performed using the transmitted part of the probe beam and those made with the reflected part have been demonstrated on bare silicon wafers, as well as measurement of effective minority carrier lifetime of a completed solar cell, demonstrating the ability of this technique to measure the effective minority carrier lifetime at any stage of the solar cell manufacturing process.

Acknowledgements

The author is grateful for the for the instruction and guidance of Dr. Rafael Kleiman, as well the entire Kleiman research group for their feedback and suggestions during the course of this research. In particular, the assistance provided by Kevin Boyd and Dr. Abhi Rampal was indispensable in the preparation and execution of the experiments discussed in this thesis. The author would also like to extend their gratitude towards Dr. George Chiran for his help in preparing laboratory space, locating components and equipment, and his well-received advice and support, as well as of Doris V. Stevanovic, Peter Jonasson, and Dr. Shahram Tavakoli for their advice and assistance in tackling problems as they arose.

Finally, the author would like to extend a great deal of gratitude to Rebekah Pater for her unconditional support and encouragement throughout the course of this research, as well as the support of friends and family without whom the author could not have completed this work.

Table of Contents

List of Figures

1. Introduction

The modern world is driven by semiconductor based devices. There is little in our lives not touched by semiconductors, from the components of our mobile devices and personal desktop computers to those supporting the larger machines of industry, and – increasingly – power generation. It follows that characterization of the physical parameters of semiconductors is paramount to ensure the necessary standards for each device are met and to optimize existing devices as well as continuing innovation.

A strong parameter in such characterization is the minority carrier lifetime – the average timescale for which an optically or electrically excited population of minority carriers will exist before recombining with majority carriers. For a given material, knowledge of this timescale allows for prediction of future device quality as well as a determination of material quality by the detection of defects such as dangling bonds at the surfaces and elemental impurities within the bulk [1]. Materials with fewer defects and trap states have a longer minority carrier lifetime than those with a greater defect density, thus measurement of this parameter allows for a method of differentiating materials of greater or lesser purity.

In determining a material's suitability for a given device, the use of this parameter is then easily seen. For instance, if a device requires high switching speeds then a material with too great a minority carrier lifetime could be detrimental. This is then valuable information to have before device manufacturing begins. Conversely, for applications such as solar panels, for which it is desirable that electrons remain in the conduction band for as long as is possible, a material with a high minority carrier lifetime is preferred. In the case of the latter, a rapidly growing demand for this technology requires that the quality of material is determined early in the fabrication process as this will ultimately minimize cost, time, and waste during fabrication, aiding in the continuing expansion of the market by driving down overall cost of production and, most importantly, allowing manufacturers to maximize the likelihood of producing a solar cell of the highest possible efficiency.

The relationship between minority carrier lifetime and efficiency of solar cells begins with the photovoltaic effect. For semiconducting materials incident photons of energy greater than or equal to the bandgap of the material are absorbed by electrons in the valence band. These electrons are then excited across the bandgap to a higher energy state in the conduction band, and importantly, remain confined to the material. Electrons in the conduction band are able to contribute to a current. Similarly, a vacancy is left behind – termed a "hole" – and this absence of charge can be treated mathematically as a particle of equal and opposite charge to the electron able to move throughout the valence band. Each particle will continue to contribute to conduction in the material until recombination with their oppositely charged peer through one of several mechanisms outlined in section 2.2.

In the fabrication of silicon based solar cells, silicon is subjected to chemical doping. A group IV element, silicon may be positively doped with a group III element – typically boron or indium – or negatively doped with a group V element – typically phosphorus or arsenic – increasing the density of positively charged holes in the valence band or negatively charged electrons in the conduction band respectively [2]. This process is performed during the growth process, and determines whether the electron or hole will be the minority carrier. The material is said to be P-type doped in the former and N-type doped in the latter.

In the absence of doping, equal densities of both holes and electrons are free to wander in the material in a random walk. The result is a low conductivity of the material. The purpose of a solar cell, however, is to produce a constant and useful voltage in the presence of solar radiation. Doping densities typically orders of magnitude higher than the intrinsic population of free carriers are used in order to increase the asymmetry in charge carriers. The electrical properties of the silicon may then be manipulated further by the introduction of a P-N junction.

A P-N junction is simply the junction between P-doped silicon and N-doped silicon. Typically the top layer, upon which the solar radiation is first incident, will be N-type silicon and be thinner than the bottom P-type layer, as seen in figure 1.1 This is

deliberate, and for two reasons. A thin top layer ensures that photons will not have to penetrate too great a distance into the solar cell in order to generate carriers on either side of the junction, and additionally, that the mobility of electrons – the minority carrier in the base – is greater than that of holes in silicon.

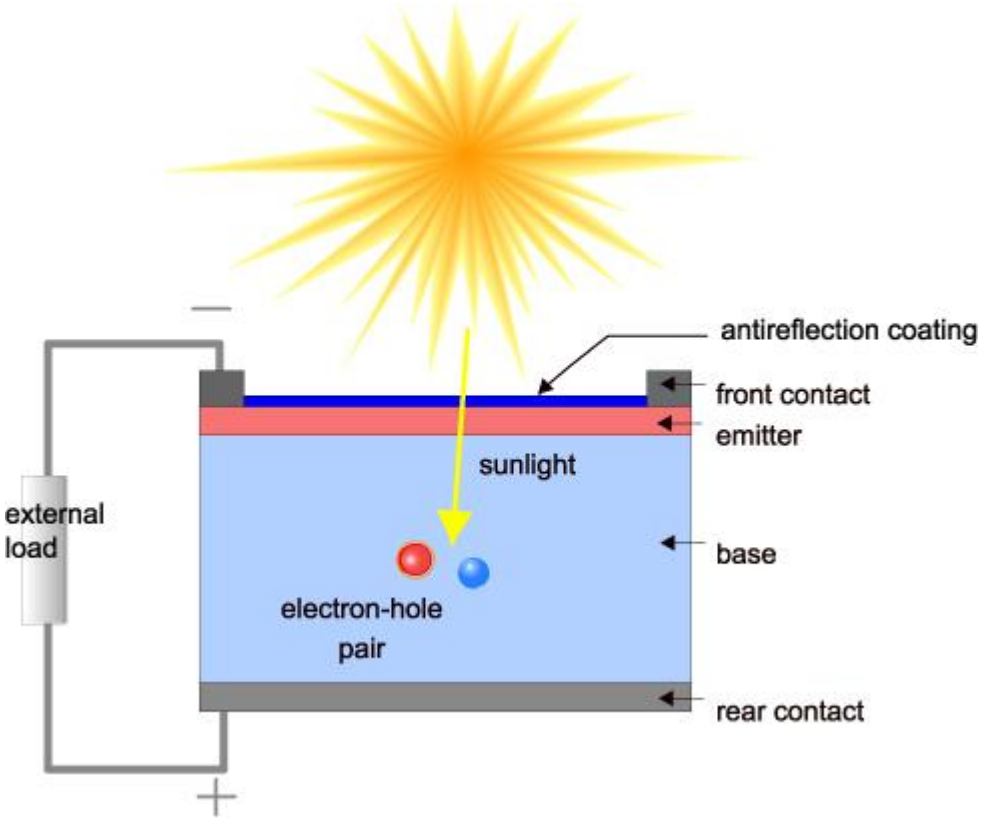

Figure 1.1 Diagram of a functional solar cell integrated in a circuit. Image from http://www.pveducation.org/pvcdrom/solar-cell-structure [3]. The emitter layer is of N-type silicon, and the base layer is of P-type silicon. An anti-reflection coating is present in order to maximize the number of light entering the cell. Minority carriers swept across the depletion region are collected by the front and rear contacts where they may complete the circuit while passing through an external load.

As seen in figure 1.1, for a solar cell in operation, photons from the sun are incident on the solar cell. Under ideal operation the broadband solar radiation is absorbed throughout the cell, and in doing do creates electron-hole pairs. Electrons, the majority carrier in N-type top layer, must travel through the silicon to a front contact, at which point they pass through the load to the rear contact where they may recombine with a

hole in the P-type base layer, completing the circuit. In both the N-type and P-type layers, minority carriers are at great risk of recombination with majority carriers before they are able to contribute to useful current in the circuit. If they are able to reach the depletion region minority carriers will be swept across the junction and become majority carriers. The more minority carriers make it across the depletion region, the greater the polarization of the cell, and the greater the total electric potential.

A high minority carrier lifetime is equivalent to a low recombination rate, and thus a high minority carrier lifetime means that, on average, a minority carrier will be able to travel further in the material, allowing for a greater chance of making it across the depletion region, being collected at a contact and, ultimately, a higher efficiency of solar cell. This is what makes the minority carrier lifetime such a valuable predictor of efficiency of the completed solar cell.

The principle methods for minority carrier lifetime determination are currently Microwave photoconductance decay (MW-PCD) and quasi-steady-state photoconductance (QSSPC). These methods are explained in greater detail in section 2.3.

Both MW-PCD and QSSPC rely on illumination of a sample by a flash bulb. Where they differ is in the timescale of illumination. In the case of QSSPC, the sample is illuminated until a steady state condition is reached between generation and recombination rates of charge carriers are equal, at which point the photoconductance is inferred from an RF coil at a known distance from the sample [4]. The minority carrier lifetime may be inferred by the methods explained in section 2.1. The chief distinction of MW-PCD is that it relies on a transient method, illuminating the sample and then examining the photoconductance decay over time [4]. The minority carrier lifetime may then be derived from this information by the methods explained in section 2.3.

Both QSSPC and MW-PCD are established methods of lifetime determination, however, the necessary hardware and data analysis of these methods, particularly in the case of MWPCD, is cumbersome.

A less ubiquitous method for lifetime determination, which has been the focus of this thesis, is measuring the modulated free carrier absorption (MFCA) of photons with

energy below the bandgap that, in the absence of free carriers, simply transmit through the material. This simple pump-probe experiment, as described in detail in section 4, relies on a laser with photon energy greater than the bandgap. This "pump" laser is absorbed by electrons in the valence band, exciting them across the bandgap and creating a population of free carriers in the conduction band. A second "probe" laser of photon energy less than the bandgap energy is passed through the sample whereupon attenuation due to free carriers occurs. The change in intensity of this probe laser due to absorption by free carriers is measured on a detector.

When the pump laser is modulated at a set frequency, the resulting generation and recombination of free carriers in the conduction band will cause the intensity of the probe laser measured on the detector to undergo a periodic decrease at the frequency of modulation. By sweeping through a sufficient range of modulation frequencies and examining the amplitude of the drop in intensity of the probe laser at each frequency, the carrier lifetime may be easily determined by fitting the amplitude of periodic intensity drop of the probe laser as a function of frequency to a lorentzian function for which the characteristic timescale is the minority carrier lifetime [5]**.** It is this method and its applications which will be the subject of this thesis.

From a production standpoint, there are immediate advantages to the MFCA method of lifetime determination. It is a truly contactless method of measurement and its set up is both simple and compact, requiring only two lasers, a method of modulation, a detector, and a lock in amplifier.

As will be shown in section 6, this MFCA apparatus is capable of measuring the minority carrier lifetime not only from the transmitted part of the probe laser, as is typical in experiments of this kind, but also from the reflected part. Additionally, the experiment is capable of collecting reflected light which is scattered off of a surface. This allows for minority lifetime measurements to be performed on textured and metalized samples. Thus, this method may be employed along any part of the production process from bare silicon to a completed solar cell. This allows for a great deal of quality control, as at each production step the solar cell may be tested to ensure there has been no degradation of

lifetime, and thus ensure a maximum efficiency of the finished product. Unlike QSSPC and MWPCD set ups, there are no dimensional requirements to hardware for this method. The pump and probe laser can be placed at an arbitrary distance to the sample allowing for greater ease in deployment. Additionally, as will be seen in section 5, data analysis is minimal, allowing for less consumption of computational power.

2. Background and theory

2.1 Recombination

Recombination of charge carriers in semiconductors occurs when an electron in the conduction band recombines with a vacancy, or hole, in the valence band. In this way, recombination may be thought of as the end of the lifetime of an electron hole pair [6]. In general, electron hole pairs can recombine via Shockley-Read-Hall, Radiative, or Auger recombination, as in figure 2.1. Which of these recombination mechanisms will dominate in a given system depends on the injection level, the purity of the semiconductor material, and whether the semiconductor is a direct or indirect bandgap material [7].

Radiative recombination occurs via an electron in the conduction band dropping down to the valence band. In order to conserve the energy of the system, a photon of energy equal to the band gap is released. Such recombination events occur much more frequently in direct bandgap semiconductors, as conduction band minimum and valence band maximum occur at the same location in k-space, and no change in momentum of recombining particles is required. Typical radiative recombination rates in direct band gap semiconductors are on the order of $10^{-10} cm^3/s$ as compared to a recombination rate on the order of $10^{-15} cm^3/s$ for indirect bandgap semiconductors such as silicon [7].

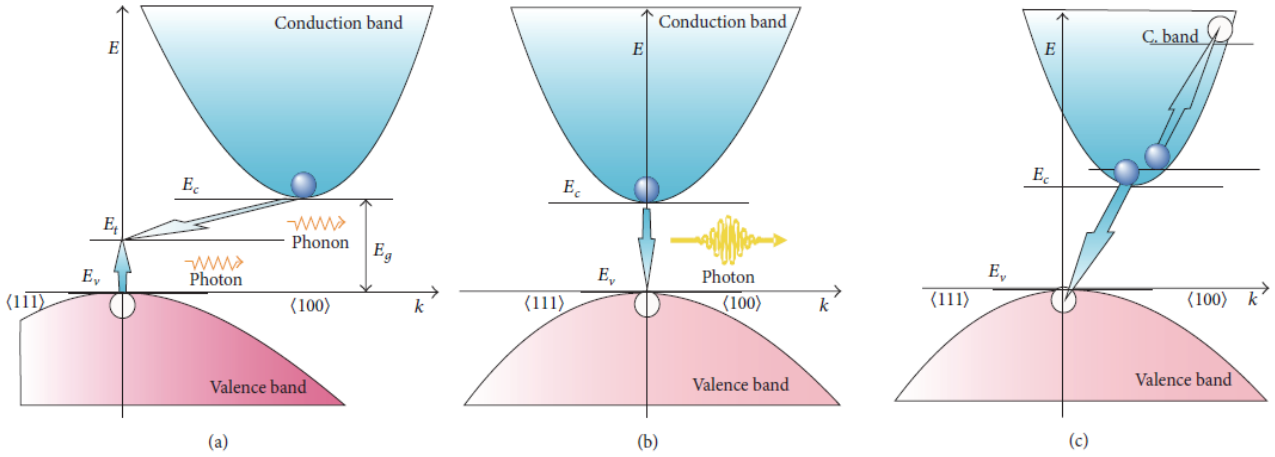

Figure 2.1: Recombination mechanisms in semiconductors. (a) Shockley-Read-Hall, or, trap assisted recombination. (b) Radiative recombination. (c) Auger recombination. [6]

Shockley-Read-Hall (SRH) recombination, also called trap assisted recombination, is the dominant recombination mechanism in indirect bandgap semiconductors and is largely due to material impurities in the bulk. These material impurities provide interstitial energy levels within the bandgap which act as more easily available recombination centers. These recombination centers act to "trap" electrons from the conduction band, which then have a higher probability to recombine with a hole in the valence band from this interstitial state [7]. In order for these transitions to occur, however, a change in momentum of the conduction band electron is still necessary. This is achieved via a heat transfer interaction with the lattice. A momentum change occurs upon an electron-phonon interaction which allows the electron to drop down to the energy level of the trap. An equivalent reaction allows a valence band hole to undergo and increase in energy sufficient to rise to the level of the trap. In this way, electron-hole pairs are able to recombine at the level of the trap state [6].

Auger recombination is a three particle process which can involve either two electrons in the conduction band and a single hole in the valence band, or two holes in the valence band and one electron in the conduction band. Due to the presence of electrons and holes at the levels of trap states, it is possible for auger recombination to occur there as well [6]. Momentum and energy transfer between electrons in the conduction band or

holes in the valence band allows for an electron to relax to the valence band in the former case or for a hole to become excited to the conduction band in the latter. In either case, the change in energy and momentum which is necessary for the electron-hole pair's recombination is transferred to a third particle, preserving the energy and momentum of the system [6].

The requirement of the interaction with a third particle means that auger recombination times will be much longer at lower free carrier densities, however, at high injection levels the increased free carrier density allows for Auger recombination events to become more frequent, decreasing the total effective lifetime of the sample.

In general, the recombination lifetime in the bulk ,τ_r, is a function of SRH, Radiative, and Auger recombination rates such that equation 2.1 below is satisfied.

$$\frac{1}{\tau_r} = \frac{1}{\tau_{SRH}} + \frac{1}{\tau_{rad}} + \frac{1}{\tau_{aug}} \tag{2.1}$$

In silicon, an indirect bandgap semiconductor, radiative recombination rates are much lower than SRH recombination rates. Below injection levels on the order of $10^{18} cm^{-3}$ [6] auger recombination rates are as well much lower than that of SRH. This of course means that below a – sample dependent – critical injection level a measurement of bulk lifetime in silicon is equivalent to a measure of the material purity.

In practice the bulk recombination mechanisms discussed above are difficult to decouple from the effects of the surface. Dangling bonds present at the surface act as efficient recombination centers for electrons and holes, and carriers generated near the surface are at great risk of becoming entrapped in these recombination centers. In thin samples, or in thicker samples with sufficiently large diffusion lengths, it is not obvious if the recombination lifetime is limited by bulk recombination processes or a high surface recombination velocity. The total recombination rate of electrons and holes in the material is then not sufficiently described by equation 2.1, and requires an additional term describing recombination rate due to the surface:

$$\frac{1}{\tau_r} = \frac{1}{\tau_{SRH}} + \frac{1}{\tau_{rad}} + \frac{1}{\tau_{aug}} + \frac{1}{\tau_{surface}} \tag{2.2}$$

2.2 Injection Level Dependence of the Effective Lifetime

The effective lifetime of a semiconductor is a vague quantity without mentioning the injection level – the average density of excess minority carriers – under which it was measured. The timescales of the recombination mechanisms discussed in the previous section are themselves dependent on the injection level, and by equation 2.2 there must then be an injection level dependence on the overall recombination lifetime in the bulk [7]–[9] and surface effects [9], and therefore on the effective lifetime of the sample.

The injection level as a general concept is simple. Under the assumption that each photon above the bandgap is absorbed and creates an electron-hole pair in the material, the injection level is proportional to the rate at which photons enter the material.

In reality, the injection level dependence of each of the recombination timescales discussed in the previous section can be complicated functions of material properties. Energy levels of interstitial traps as well as dopant type and density may affect the overall dependency of τ_{eff} on injection level [7], [9], [10], however, some general remarks can be made.

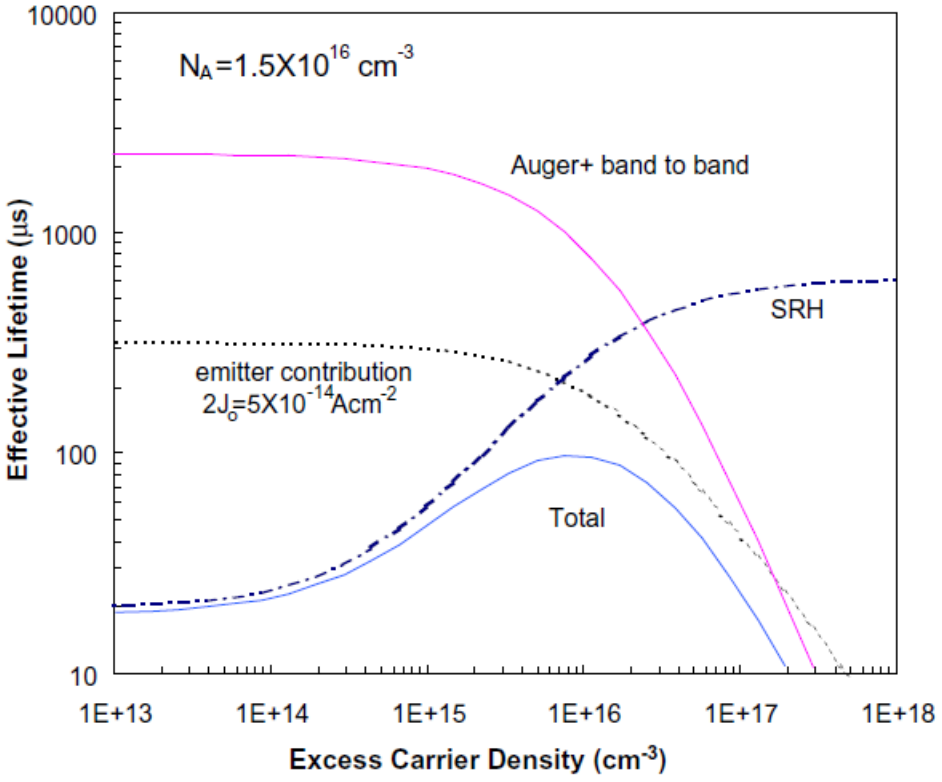

Figure 2.2: Recombination lifetimes as a function of excess carrier density. Auger, band to band radiative recombination and SRH are described in section 2.1. The emitter contribution is a surface effect due to the presence of dopant diffusions at the surface. The total effect is a decrease in effective lifetime at high injection levels [9].

Figure 2.2 shows the dependency of recombination lifetimes on injection level as well as the sum total of these lifetimes, or τ_{eff}. As the excess carrier density, Δn, increases with higher injection and approaches the background carrier concentration of the material, τ_{SRH} increases causing τ_{eff} to increase as well. One would expect this dependence on τ_{SRH}, as the increase in carrier density leads to saturation of trap states.

The increase in Δn , as discussed in the previous section, leads to an increase in the frequency of Auger recombination. Beyond a critical injection level, Auger recombination becomes the dominant recombination mechanism, and despite the increase

in τ_{SRH}, the low τ_{aug} will be the dominant contribution to τ_{eff}. By equation 2.2, τ_{eff} must then decrease proportionately.

Observing the effect of injection level on the total effective lifetime in figure 2.2, the importance of quoting an injection level alongside a measured effective lifetime becomes particularly apparent. The increase in effective lifetime due to saturation of trap states is responsible for an initial rise in τ_{eff} before the high injection τ_{aug} causes it to undergo a steep drop off. In this way, the same value of t_{eff} may be measured at injection levels several orders of magnitude apart yet give no information about the material parameter that happens to be limiting τ_{eff}.

2.3 Non-contact optical methods

The two principle non-contact methods of lifetime spectroscopy are microwave photoconductance decay (MW-PCD) and quasi steady state photo conductance (QSSPC). Both are well established as optical methods for semiconductor characterization [11] [12], although the two optical techniques take advantage of distinct timescales of illumination.

In general, non-contact optical methods fall in to one of the following three regimes of illumination: A sharp impulse of light, a steady state illumination of the sample, and a quasi-steady state illumination in which the intensity of illumination gradually decreases to zero over a timescale of milliseconds[4], [13]. The first of these regimes is used in the transient technique in which the decay of the carrier density after illumination can provide information about the free carrier lifetime [4]. Microwave PCD operates in this regime.

The steady state illumination regime is not ideal for determination of free carrier lifetime due to the heating of the sample, which in turn alter its material properties and introduce undo errors in to the measurement. The third is the quasi-steady state regime, in which a constant illumination source is present but the intensity fades over a sufficient

timescale that heating effects are not significant to alter material properties [4]. QSSPC measurements occur in this regime so as to avoid the heating issues inherent in the true steady state regime.

To understand the physics behind both methods, we begin with the general continuity equation for all three timescales of illumination[4], [13].

$$\frac{\partial \Delta n}{\partial t} = G_b(t,x) - U_b(t,x) + \frac{1}{q}\frac{dJ_n}{dx}, \tag{2.3}$$

where $G_b(t,x)$ and $U_b(t,x)$ are the respective generation and recombination rates in the bulk, Δn is the excess minority carrier density, and J_n is electron current density.

Nagel et al. [14], considering the general continuity equation, combine the bulk and surface recombination effects into a single, effective, recombination rate, U_{eff}, which satisfies equation 2.3. From U_{eff} Nagel et al. determine an effective timescale of recombination, τ_{eff}, which combines information about bulk and surface recombination into a single general parameter

$$\tau_{eff} = \frac{\Delta n_{avg}(t)}{G_{avg} - \frac{\delta \Delta n_{avg}(t)}{\delta t}}. \tag{2.4}$$

n_{avg} and G_{avg} are the average excess carrier density and generation rate respectively, integrated over the thickness of the sample. Note that equation 2.4 is valid for any interval of illumination decay.

In the transient case the generation rate is zero and equation 2.4 becomes

$$\tau_{eff} = \frac{\Delta n_{avg}(t)}{\frac{\delta \Delta n_{avg}(t)}{\delta t}}. \tag{2.5}$$

Under steady state and quasi steady state conditions $\delta\Delta n_{avg}(t)\delta t = 0$, and equation 2.4 becomes

$$\tau_{eff} = \frac{\Delta n_{avg}(t)}{G_{avg}}. \tag{2.6}$$

2.3.1 QSSPC

The effective lifetime in the quasi-steady state photo conductance method is given by equation 2.5 above. This is a special case of equation 2.4 in which Δn is kept constant under illumination, and thus the second term in the denominator of equation 2.4 goes to zero. The average excess minority carrier density under quasi-steady state illumination is

$$\Delta n_{avg} = \frac{\Delta\sigma(t)}{q(\mu_n+\mu_p)W}\ , \tag{2.7}$$

where σ is the pre-determined excess photo conductance of a sample, μ_n and μ_p are the electron and hole mobilities respectively and W is the thickness of the sample [4].

The Generation rate will depend on the number of photons absorbed by the material. While below a critical injection level, it is assumed that one absorbed photon will excite a single electron across the band gap and create a single electron hole pair. The generation rate is then

$$G_{avg}(t) = \frac{I_{av}(t) f_{abs} N_{ph}^{1sun}}{W}. \tag{2.8}$$

where I_{av} is the average number of photons incident on the sample surface, f_{abs} is the fraction of photons absorbed by the sample, N_{ph}^{1sun} is the photon flux in units of 1 sun,

and W is the thickness of the sample [4]. $G_{avg}(t)$ and Δn_{avg} can determined by a device capable of measuring QSSPC, and t_{eff} can be calculated by equation 2.6.

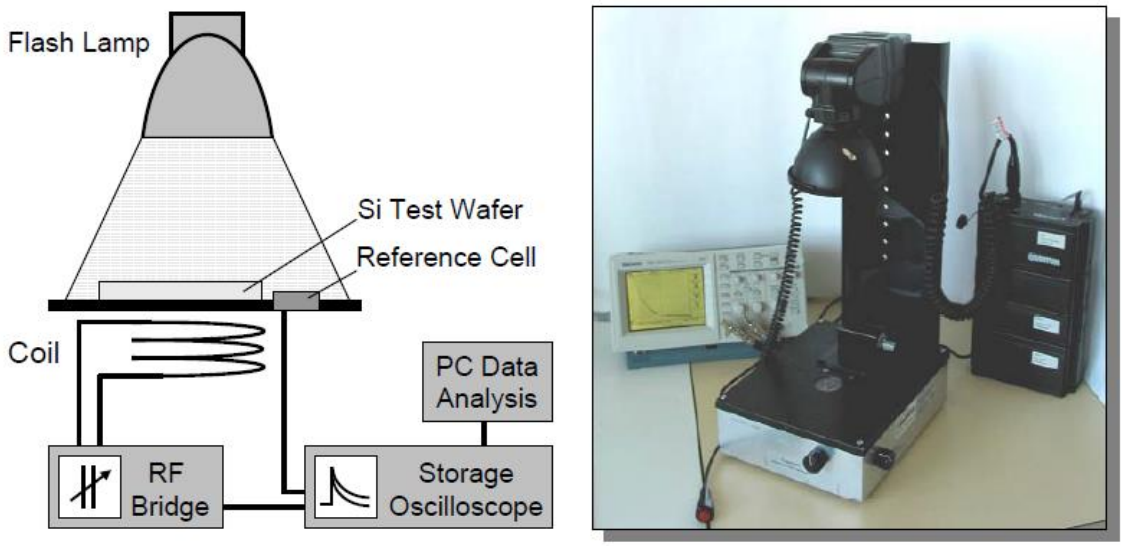

Figure 2.3: The Sinton QSSPC measurement system. Consisting of an RF bridge, a conductive coil, and a flash lamp, this system is capable of measuring injection dependent carrier lifetimes of semiconductor wafers[4].

The Sinton, seen in figure 2.3 is such a device. The Sinton makes use of a flash lamp as an illumination source, and an RF bridge coupled inductively to the sample with a conductive coil. The measured change in conductance of the sample is used to determine $G_{avg}(t)$ and Δn_{avg} experimentally, from which an effective minority carrier lifetime of the sample is determined.

The QSSPC measurement capabilities of the Sinton allow for determination of effective lifetime ranging between 0.1 μs to milliseconds, and can be used accurately over a range of injection levels from $10^{12} - 10^{17} cm^{-3}$ [4].

2.3.2 MW-PCD

The effective lifetime may be determined by MW-PCD by measuring the change in microwave reflectance of a sample due to the decay of photoconductance after an illumination pulse.

A block diagram of the MW-PCD system at the Fraunhofer Institute for Solar Energy is shown below in figure 2.4. A pump laser, of photon energy above the bandgap, generates a population of electron-hole pairs in the material. 2.8 GHz microwaves are passed through an attenuator before being split equally across two branches. Half of the microwave radiation is directed towards the sample via an antenna, whereupon the reflected part of the microwave radiation is recombined with the other half which has been passed through a variable phase shifter and attenuator. The ability to adjust the phase and attenuation of the half of the microwave radiation which does not interact with the sample allows for subtraction of the time independent portion, leaving only the time dependent signal generated by the change in photoconductance of the sample due to the illumination pulse of the pump laser [4].

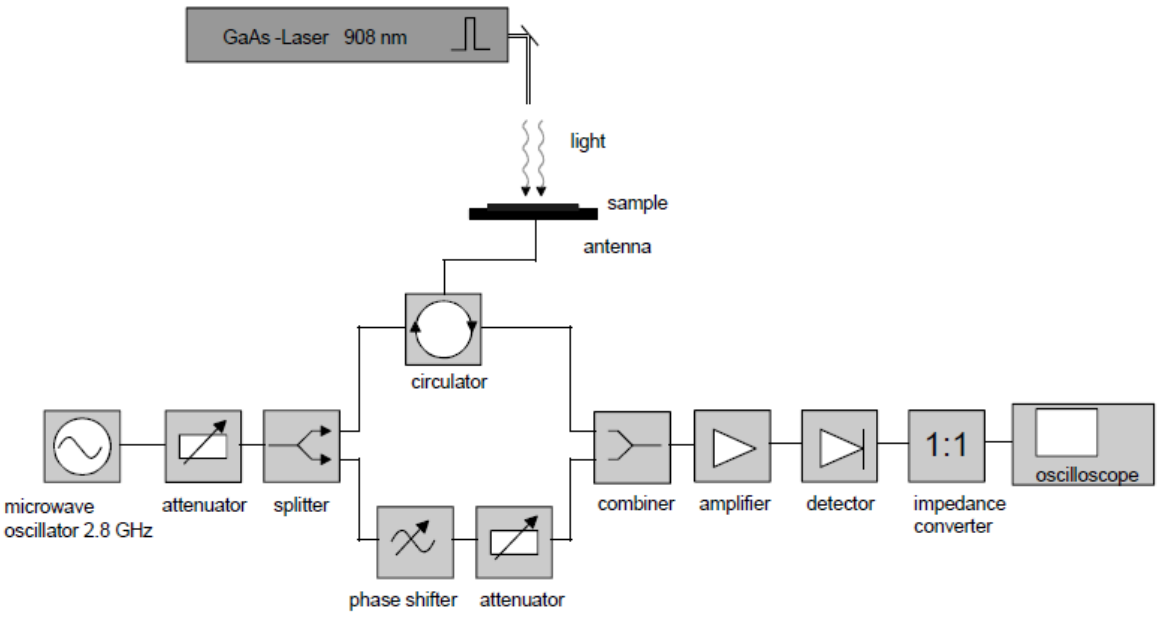

Figure 2.4: Block diagram of the MW-PCD system at the Fraunhofer Institute for Solar Energy [4].

Under low injection levels, the measured decrease in photoconductance is proportional to the rate of recombination of electron-hole pairs, and the effective lifetime of the sample can be determined quite simply [15]. By measuring the timescale of the photoconductance decay after illumination has ceased, the derivative with respect to time of equation 2.7 is determined. The effective lifetime may then be calculated from equation 2.5 [4].

Measurement of effective lifetime by MW-PCD at high injection levels requires more care than low injection level measurements. The proportionality between photoconductance of the sample and carrier concentration is valid only for small changes in photoconductance of the sample, beyond which the microwave reflectance becomes a non-linear function of the sample conductivity[15]. In order to perform a measurement at high injection levels a calibrated bias lamp is used to generate the desired background concentration of free carriers. The pump laser then excites a population of free carriers which is small compared to the background concentration. So long as the illumination from the bias lamp remains constant the change in carrier density due to the pump laser is small compared to the background concentration, satisfying the conditions for linearity in microwave reflectance [4].

While the bias lamp allows for high injection level measurements, measurements of effective lifetime obtained under illumination of a bias lamp are actually measurements of the differential lifetime

$$\tau_{diff} = \frac{\partial \tau_{eff}}{\partial \Delta n}. \tag{2.9}$$

In order to determine the true effective lifetime, the differential lifetimes must be integrated over all injection levels below the injection level of the desired measurement [4] [16].

2.3.3 Pump-Probe

A third non-contact, optical, method of effective lifetime determination is the pump-probe method. Our description of it here will be necessarily brief, however an in depth explanation of pump-probe methodology is given in the following section.

Pump-probe measurements, as described previously, rely on a "pump laser" of photon energy greater than the bandgap to excite populations of free carriers in semiconductor sample, while a "probe" laser of photon energy less than that of the bandgap is allowed to pass through the sample whereupon its intensity is monitored by a detector. As free carriers are created in the sample, photons from the probe laser are absorbed by the free carriers such that the change probe intensity, I_{probe}, is proportional to the change in excess density of free carriers. By monitoring the intensity of the probe, the change in excess carrier density of the material may be monitored.

$$\Delta I_{probe} \propto \Delta n \tag{2.10}$$

The pump laser may illuminate the sample in any of the illumination timescales discussed above, which allows for the possibility of both QSSPC [17] and transient measurements [8] to be performed with methods similar to those given above.

Rather than observing the change of I_{probe} over time directly, measurements may instead be made in frequency space. It is trivial to show that periodic modulation of the pump laser at frequency f excites a free carrier population in the sample at the same frequency. Thus, I_{probe} will undergo a periodic attenuation at frequency f. This periodic attenuation is measured on a lock in amplifier as in figure 4.1.

The length of time that excess carriers exist in the material before recombination is, of course, τ_{eff}. If τ_{eff} is smaller than $1/f$ there will be a periodic attenuation of the probe laser of amplitude A_0. As $1/f$ becomes smaller than τ_{eff} the periodic amplitude

of attenuation A_f will be smaller than A_0 as each population of free carriers will be generated before recombination of the preceding population, and thus I_{probe} as measured on the detector will not have been able to recover to its initial intensity. As frequency of modulation is increased, the periodic amplitude of the change in probe laser intensity will decrease such that

$$A_0 > A_{f_i} > A_{f_{i+1}} \quad . \tag{2.11}$$

The decrease in amplitude of attenuation is fit to a lorentzian roll off,

$$\Delta I_{probe}(f) = \frac{A_o}{\sqrt{1+\left(2\pi f \tau_{eff}\right)^2}} \tag{2.12}$$

for which the shape of the curve is uniquely determined by τ_{eff}. Examples of such curves resulting from experiment may be seen in sections 5 and 6.

3. Literature Review

3.1 introduction

Throughout the twentieth century the electrical transport properties of semiconducting materials was a growing field of study. The mid-century boom of metallurgy and the increase in utilization of more complex ternary and quaternary alloys as well as the adoption of semiconducting materials in the machines of industry – such as the silicon transistor replacing the cathode ray tube in electronic computers – increased the need for optimization of such materials. In order to optimize the physical characteristics of a semiconductor for device specific use, however, it was necessary to devise methods to accurately characterize the physical properties.

As argued in section 1 above, understanding the dynamics of charge carriers in semiconductors, such as minority carrier lifetime, mobility, and diffusion length are paramount if one's goal is to optimize a material to a specific use. To that end, much work was done to determine efficient methods of studying such properties. It was perhaps a natural inclination to study these electrical properties through tests relying on electrical conduction, however, these methods require contact with the material which often results in degrading effects. Early in the second half of the century, as photovoltaics was beginning to move from the domain of military study to civilian and industrial applications, opto-electronic techniques to characterize materials began to emerge. Relying on study of the interactions of photons and charge carriers, some of these opto-electric methods had the benefit of being non-contact, and thus avoided the issue of degradation. In particular the observation that free carriers in the conduction band are able to interact with photons with sub-bandgap energies has opened the door to a class of truly contactless electrical measurements.

In the latter half of the twentieth century, free carrier absorption measurements were not, on their own, novel. In a 1978 paper, for example, Schroder et al. discuss the problems of attenuation of long wavelengths due to FCA in extrinsic silicon IR detectors. Though a thorough investigation in to the parasitic effects of FCA is given, the authors stop short of concluding the potential for FCA as a tool for characterizing MCL [18]. Two years earlier, Houston and Krishna published a paper in which FCA is used as a diagnostic tool to measure the density of minority carriers in a semiconductor device [19], and as early as 1956 N.J Harrick published a paper demonstrating the capability of (unmodulated) free carrier absorption measurements to determine the lifetime of excess carriers in the bulk of a germanium sample [17]. Although the foundation for FCA as a method of minority carrier lifetime was presented in this paper, there were few publications of papers employing this method over the next several decades. It was not until the end of the 1980's that this method seems to have become more widely adopted, and, in particular, progressed towards modulating the injection of free carriers rather than relying on measurements made at steady state conditions. It is this particular non-contact

method which is the topic of this thesis, and the history of this technique will be explored below before continuing in the discussion of the author's own research.

3.2 Notable work

3.2.1 FCA

N.J Harrick's work in 1956 [17] demonstrates a truly contactless technique for determining bulk carrier lifetimes in semiconductors by observing the attenuation of an infrared light source by free carriers injected via a constant source of visible light as seen in figure 3.1 below.

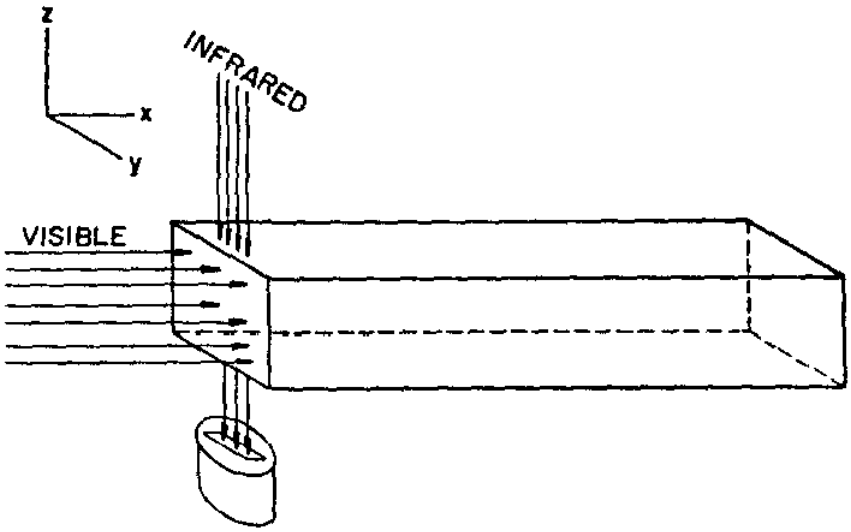

Figure 3.1: Harrick's experimental set up. IR light enters a Germanium sample perpendicular to the unmodulated pump light. This ensures that it passes through a volume of even carrier density. A detector is placed on opposite side of sample to monitor attenuation of IR radiation due to free carriers excited by the visible radiation [17].

A shutter between the visible "pump" radiation and the sample is opened for a sufficient time that the system is able to achieve a steady state, at which time the shutter

is then closed. Although the pump is not modulated, its presence in this FCA experiment is what allows the measurement to be made in a contactless fashion. The surfaces are etched in order to suppress surface recombination velocity (SRV), and as a secondary precaution, the uniformity of the visible radiation's illumination through the width of the sample allows for the majority of the attenuation of the IR to occur in the bulk [17]. Harrick demonstrated this technique for several samples of germanium.

Under the assumption that SRV is negligible, Harrick's lifetime measurements are made when the system reaches steady state, as mentioned above. Neglecting traps and the electric field term, the steady state continuity equation is as follows:

$$D\,\frac{\partial^2 \Delta p}{\partial x^2} = \frac{\Delta p}{\tau}\,, \tag{3.1}$$

where τ is the free carrier lifetime, Δp is the excess free carrier density, and D is the ambipolar diffusivity which is given by

$$D = (n+p)/(\frac{n}{D_p} + \frac{p}{D_n}), \tag{3.2}$$

where n and p are, respectively, the electron and hole densities and D_n and D_p are the diffusivities of electrons and holes respectively. Further, the carrier lifetime τ is given as

$$\tau = \tau_o(1 + a\Delta p)/(1 + c\Delta p), \tag{3.3}$$

where τ_o is the low injection level lifetime, $c = (n_o + p_o)^{-1}$, and a is dependent on the low injection level lifetime for highly doped materials [7].

By constraining the area to be sufficiently small that τ and D are constant throughout, then a local solution to 3.1 may be given as:

$$\Delta p = \Delta p_o e^{-\frac{x}{L}}, \tag{3.4}$$

where L is the diffusion length given as

$$L = \sqrt{D\tau} = \sqrt{D\tau_o(1 + a\Delta p)/(1 + c\Delta p)}. \tag{3.5}$$

There are two methods in which lifetime of excess carriers are determined. The first comes directly from measuring the attenuation of infrared radiation when the shutter blocking the visible is opened. Since the change in intensity of the IR is proportional to Δp, measuring the attenuation and employing equation 3.4 allows for a value of diffusion length to be determined. Then plugging in the value for D –as calculated in equation 3.2— into equation 3.5, the value of τ may be determined.

Additionally, lifetime measurements may be determined from equation 3.3. Values for a in equation 3.3 may be calculated from the slope of the plots in figure 3.2, in which $\frac{\tau}{\tau_0}(1 + \frac{\Delta p}{n_0+p_0})$ is plotted against Δp .

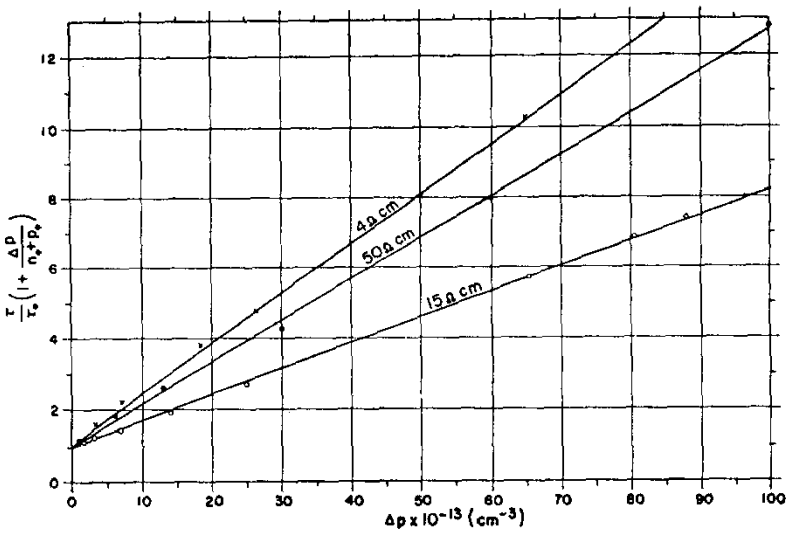

Figure 3.2: the constant, a, is determined by the slope of the curves shown for three samples of germanium to be used in 3.3 to determine sample lifetime [17].

ρ	type	τ_0	c^{-1}	a^{-1}	τ_∞
50	p	950	4.9×10^{13}	8.5×10^{13}	550
15	n	760	10×10^{13}	13.9×10^{13}	550
4	n^b	35	38×10^{13}	6.7×10^{13}	200

Table 3.1: characteristics and measured parameters of three germanium samples. Values shown are, in order from left to right: resistivity, sample type, low level lifetime, the constants c and a, and the high level lifetime [17].

A table of material parameters measured by Harrick's experiment can be seen in table 3.1.

3.2.2 MFCA

An experiment designed and implemented at Perdue University by Sanii et al. in 1988 [20] allowed for measurements of bulk lifetime of minority carriers and the surface recombination velocity (SRV) of a silicon wafer based on measurements of free carrier absorption by an infrared probe beam. Like Harrick's work, this experiment is contactless and relies on measuring attenuation of the probe beam, however, the stimulation from the pump beam is modulated across a range of frequencies. As will be shown, this modulation of frequencies leads to a comparatively simpler method for determining recombination time in the sample.

This technique, dating back to the late 1980's, is intended to be used in order to determine if degradation of the minority carrier lifetime has occurred at different processing steps involved in silicon solar fabrication. As the technique is purely optical – and thus contactless – samples may be examined at nearly any stage of processing without introducing additional hardware necessary for –what was then—traditional test apparatus which introduce their own degrading effects on the sample that cannot be reliably decoupled from the effects of individual processing steps [20]. Curiously,

however, this technique does not seem to have had the impact of either QSSPC or MW-PCD.

The experimental set up, seen in figure 3.3, is very similar to that which has been employed in our own pump-probe MFCA experiment. A pump laser of $\lambda_{pump} = 0.514\ \mu m$ is used to generate populations of free carriers and the periodic attenuation of a probe laser of wavelength $\lambda_{probe} = 3.39\ \mu m$ is measured by a detector fed to a lock in amplifier. Interestingly, the diagram shown here employs a reflection mode geometry in order to measure the probe beam. Although the data presented in this paper is from a single pass transmission mode geometry, as seen in figure 3.4, several geometries for probe beam coupling are suggested, including one intended to measure the reflected part of the beam as seen in figure 3.5.

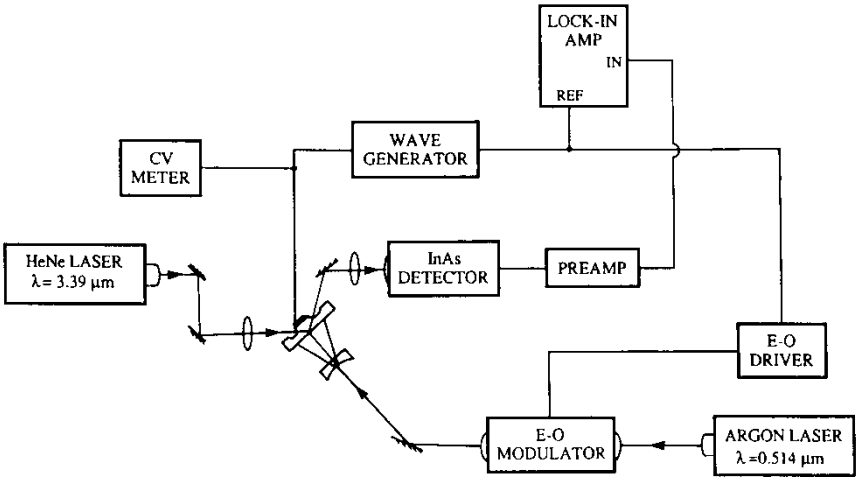

Figure 3.3: Block diagram of Sanii's MFCA experimental setup. A reflection mode geometry is shown here, however, the experimental results shown in this paper are for a single pass transmission mode geometry (figure 3.4). It seems that the reflection mode geometry was never used [20].

The stated goal of this experiment is to be able to measure SRV and bulk lifetime of wafers that are either partially or completely processed wafers [20]. Sanii et al did not appear to pursue the reflection mode geometry.

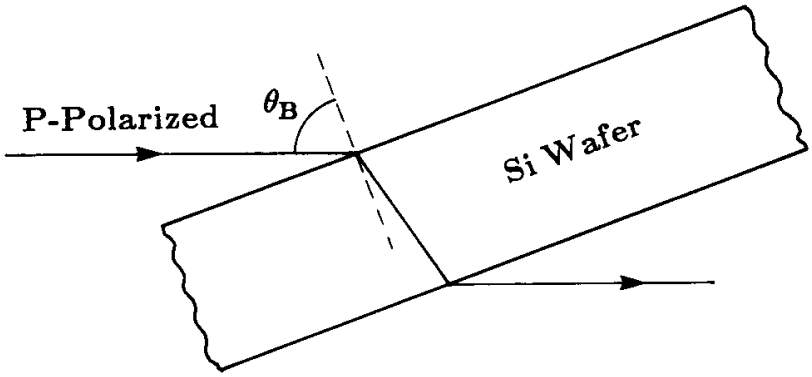

Figure 3.4: Single pass coupling of probe beam employed in the experiment by Sanii et al. An incoming probe beam at angle θ_B passes through the Si wafer. The attenuation of the transmitted part of the probe beam due to FCA is measured.

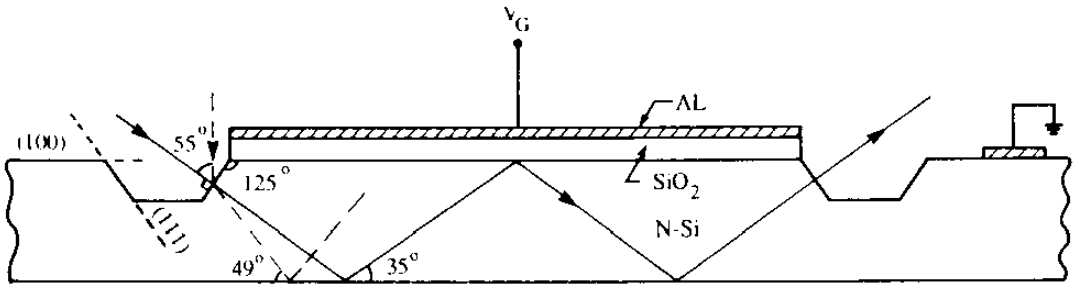

Figure 3.5: A potential probe coupling geometry proposed by Sanii et al. V-grooved etched windows allowing for the probe beam to be coupled into and back out of the same surface of the wafer. A <100> silicon wafer would be used, with the V-groove faces along the <111> plane [20].

Distinct from the steady state system which Harrick studied, in the modulated free carrier absorption (MFCA) system the generation rate is non zero and the carrier concentration is not constant. As such, the continuity equation contains additional terms:

$$D\frac{\partial^2 \Delta p}{\partial x^2} - \frac{\Delta p}{\tau} + G(x,t) = \frac{\partial \Delta p}{\partial t}. \tag{3.6}$$

Δp is the minority carrier concentration, G is the generation rate of the minority carriers, D is the diffusivity, and τ is the effective minority carrier lifetime.

Equation 3.6 is subject to the boundary conditions:

$$D\frac{\partial^2 \Delta p}{\partial x^2}|_{x=0} = S_L \Delta p(0) \tag{3.7}$$

$$D\frac{\partial^2 \Delta p}{\partial x^2}|_{x=0} = S_D \Delta p(W) \tag{3.8}$$

where S_D and S_L are the dark and illuminated sides of the sample respectively, and W is the thickness of the sample.

The generation rate is given as:

$$G(x,t) = \eta\alpha(1-\mathrm{R})\phi(\mathrm{t})e^{-\alpha x} \tag{3.9}$$

where η is quantum efficiency, $\phi(t)$ is the pump beam flux density and α is absorption coefficient at the pump wavelength.

Under the assumption that the generation rate of excess electrons and holes is equivalent and constricting $\phi(t)$ to be a periodic function in time, Sanii derives a periodic concentration of excess minority carriers, ΔP, as well as a periodic change in intensity of the probe beam [20]:

$$I = I_o\left(1 - \frac{\nu}{\cos\theta}(\sigma_n + \sigma_p)\Delta P\right) \tag{3.10}$$

where I_o is the initial intensity, ν is the number of passes the probe beam makes through the material, σ_n and σ_p are the electron and hole densities respectively, and θ is the internal reflection angle.

Sanii et al. suggest three frequency ranges for which the effective diffusion length

$$L_m = \left(\frac{D_p\tau_p}{1+im\omega\tau_p}\right)^{1/2}, \tag{3.11}$$

of minority carriers allows for measurements to be made of principally SRV, or principally the bulk lifetime. These regions are:

$$L_m = \begin{cases} (D_p\tau_p)^{\frac{1}{2}} = L_p, & \omega\tau_p \ll 1 \\ \left(\frac{D_p\tau_p}{1+im\tau_p}\right)^{1/2}, & \omega\tau_p \approx 1 \\ (1-i)\left(\frac{D_p}{2m\omega}\right)^{\frac{1}{2}}, & \omega\tau_p \gg 1 \end{cases} \tag{3.12}$$

ω in equations 3.11 and 3.12 is the angular frequency of modulation, and D_p and τ_p are the diffusivity and lifetime of minority carriers respectively.

Recall that the pump laser has a wavelength of $\lambda_{pump} = 0.514\mu m$. This allows Sanii et al. to operate under the assumption that the majority of free carrier excitation occurs near the illuminated surface, as some 95% of the incident radiation from the pump will be absorbed within the first 3 μm of material. It follows that free carriers in the bulk or near the unilluminated surface arrive there via diffusion [20]. For low frequencies, when $\omega\tau_p$ is very small, the effective diffusion length is large – equal to the diffusion length of minority carriers. In this frequency region, minority carriers may be detected in the bulk as well as at the far surface of the material. As the frequency of modulation increases, and $\omega\tau_p$ becomes large the effective diffusion length decreases, thus detection of minority carriers will be limited to the bulk and illuminated surface. As the modulation frequency increases to $\omega\tau_p \gg 1$ the effective diffusion length becomes sufficiently small that the experiment is essentially measuring only SRV of the illuminated surface, as the minority carriers will not be able to diffuse away from the surface during their lifetimes.

As the modulation of the pump beam is periodic, the decrease in intensity of the probe beam will necessarily share the same periodicity. This periodic attenuation of the

probe beam will be small compared to its initial intensity and is best measured by a lock in amplifier.

A derivation of the signal one should expect to detect on the lock in amplifier for this experiment for measuring both SRV and bulk minority carrier lifetime is derived by Sanii et al. As the measurement of SRV is not applicable to the contents of this thesis, the derivations are not shown here, although the interested reader may find them in reference [20]. Of interest is the expected amplitude of periodic attenuation of the probe beam, A, from the lock in amplifier in the special case that the SRV at both the illuminated surface and the dark surface are zero – I.e. $S_D = S_L = 0$. This results in an expected amplitude

$$A = \frac{C_o \tau_p \left(1 - e^{-\alpha W}\right)}{\sqrt{1 + \omega^2 \tau_p^2}}. \tag{3.13}$$

Equation 3.13 takes the form of a simple first order roll of filter with a proportionality constant C_o containing information about the intensities of the pump and probe beam.

The amplitude data from the experiment performed in a single pass, transmission mode geometry is shown in figure 3.6 below.

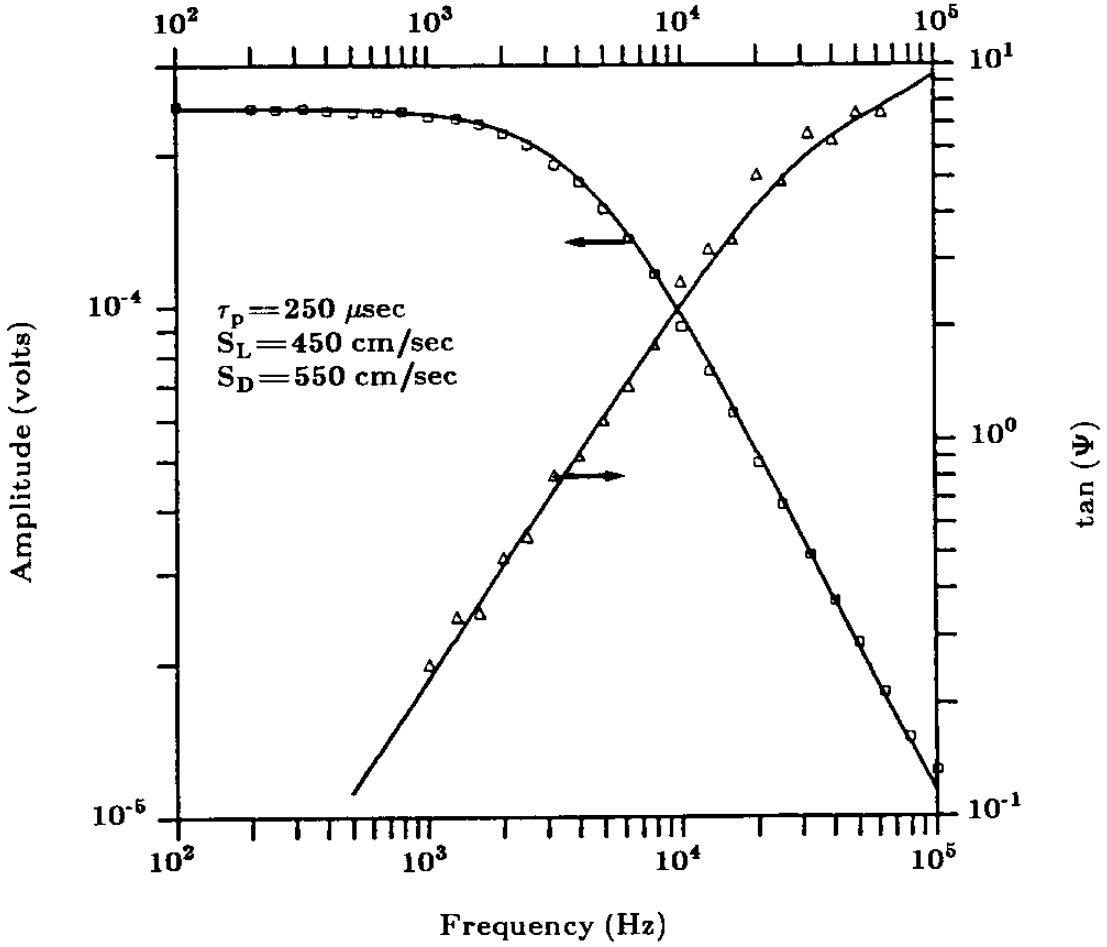

Figure 3.6: Data from the MFCA experiment of Sanii et al. performed in single pass geometry. The leftmost curve is the amplitude data A seen in equation 3.13. The leftmost curve is measured SRV as discussed in [20].

In the low frequency regime, $\omega\tau_p \ll 1$ the amplitude, A, is constant. As frequency increases, however, a decrease of 20dB/decade occurs. The frequency at which a 3dB decrease from the amplitude in the low frequency regime occurs can be used to determine the minority carrier lifetime τ_p:

$$\tau_p = \frac{1}{\omega_{3dB}}. \tag{3.14}$$

Any additional decrease in A beyond 20dB/decade is attributable to the presence of a non-zero SRV [20]. Thus this model may be used to fit the data of a sample where SRV ≠ 0, however, the lifetime measured will be an effective lifetime containing information about both SRV and bulk lifetime, the contributions of which are difficult to decouple.

3.2.3 Pump-Probe Transient

In the above discussion of pump-probe measurement techniques the data is analyzed in frequency space, however, measurements of effective lifetime and other material parameters may also be performed by examining the transient change in intensity of the probe beam due to FCA immediately following a pulse of illumination from the pump beam. In a 1998 paper [8], Jan Linnros reviews and critiques this technique and its merit as a method for free carrier lifetime determination, offering his own experimental data.

The experimental set up, seen in figure 3.7, for measuring the transient effect of FCA is similar to that of the MFCA discussed in the previous section. The major difference being that, rather than modulating the pump beam across a range of frequencies, the modulation of the pump is held at a single frequency. It is the timescale of the decay of the FCA that occurs between pulses of the pump beam that is analyzed, rather than the composite of attenuation due to FCA across a range of frequencies.

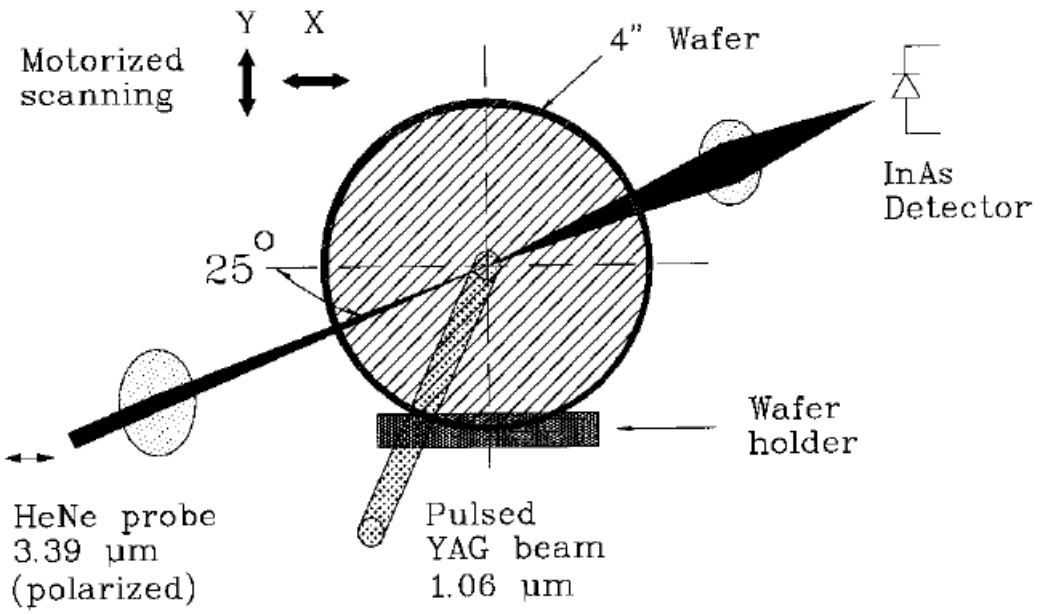

Figure 3.7: Linnros' experimental setup. A silicon wafer sits in a motorized wafer holder and is periodically illuminated by a pump beam of wavelength $\lambda_{pump} = 1.06\ \mu m$. A probe beam of wavelength $\lambda_{probe} = 3.39\ \mu m$ constantly illuminates the sample, such that the pump and probe beams illuminate the same area of the sample. A InAs detector is placed behind the sample to measure the intensity of the probe beam [8].

The number of free carriers generated in the material as a function of time and depth can be written as

$$g(x,t) = g_0(t)\frac{\alpha_{exc}(1-R)^2\exp(-x\alpha_{exc})}{1-R^2\exp(-2x\alpha_{exc})} \tag{3.15}$$

where g is the number of free carriers, x is depth in the sample, α_{exc} is the absorption coefficient of the pump beam, R is the reflection coefficient, and $g_0(t)$ is the incident photon density in the material [8]. The generation is due a pulse from the pump laser: a YAG laser of wavelength $\lambda_{pump} = 1.06\ \mu m$. The choice of a pump laser wavelength so close in photon energy to the bandgap is to ensure uniform generation of free carriers throughout the depth of the material.

The probe beam is a HeNe laser with a wavelength of $\lambda_{probe} = 3.39\ \mu m$. The intensity of the probe beam, as a function of time, due to FCA is given as

$$I(t) = I_o \exp(-\alpha_{probe}(t)d) \tag{3.16}$$

where I is the intensity of the probe beam, I_o is the incident beam intensity, d is the thickness of the sample, and α_{probe} is given by

$$\alpha_{probe}(t) = \alpha_o + \alpha_{FCA}(t) \tag{3.17}$$

where α_o is material dependant, constant, absorption coefficient, and $\alpha_{FCA}(t)$ is the absorption coefficient due to the density of free carriers in the material[18] and is given as

$$\alpha_{FCA}(t) = \sigma_{FCA}\Delta n(\mathrm{t}) \tag{3.18}$$

where Δn is the excess free carrier density, and σ_{FCA} is the free carrier absorption cross section, for which details may be found in reference [21]. In this paper, Linnros has used a value of $\sigma_{FCA} = 2.5x10^{-17}cm^2$ [8].

Given equations 3.17 and 3.18, $\Delta n(t)$ may then be determined experimentally via equation 3.16. Once the change in excess carrier concentration with time is determined, the effective lifetime may then be calculated in the same fashion as the MW-PCD transient technique in discussed in section 2.3.2:

$$\tau_{eff} = -\frac{\Delta n}{\frac{\partial \Delta n}{\partial t}} \quad . \tag{3.19}$$

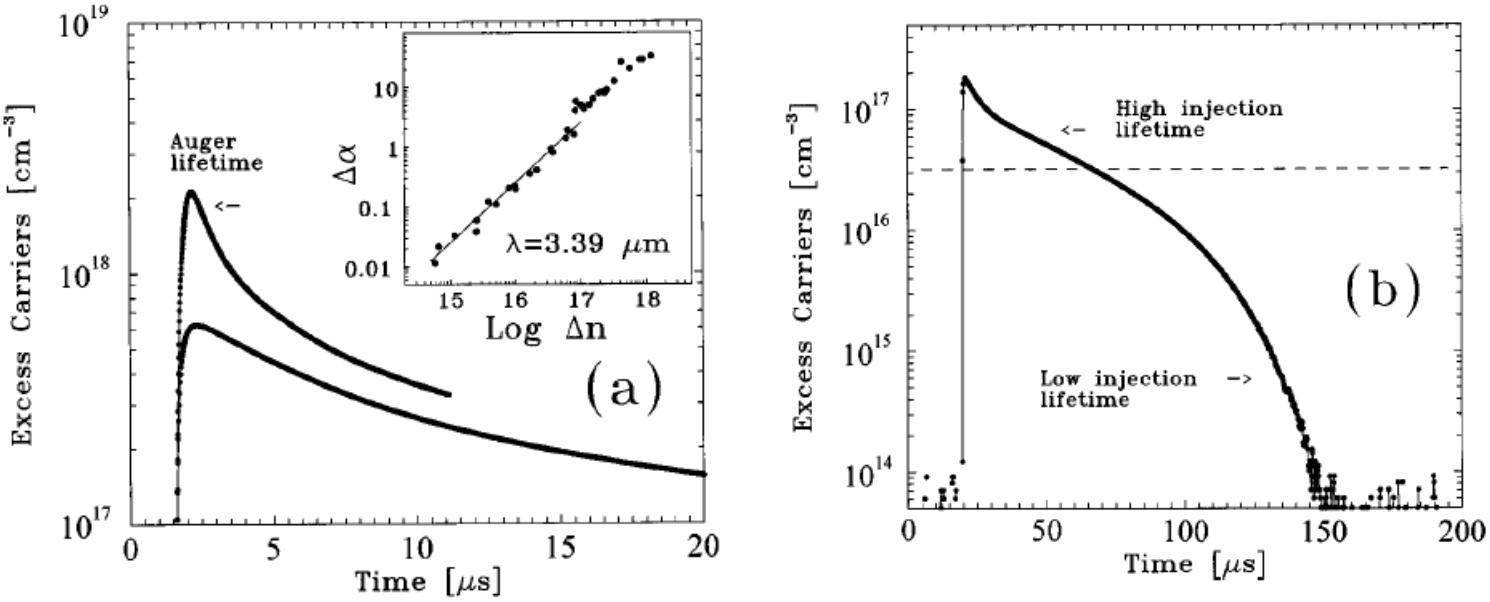

Figure 3.8: Measurements of excess carrier concentration vs time performed by Linnros. The sample is a p-type Si:B wafer with $3.2x10^{16}cm^{-3}$ dopant density of orientation <100> and thickness of $430\ \mu m$. The sample has been passivated by oxidation at 1100 degrees for a period of two hours. A 300 ns excitation pulse is used. Figure (a) shows transients at two different injection levels, displaying that the auger limited lifetime can be measured as well as lifetime at lower injection levels. (b) displays a longer observation of the high injection level excess carrier decay [8].

Experimental results of excess carrier concentration vs time can be seen in figure 3.8. Figure (a) displays two transients. At an injection level $> 10^{17}cm^{-3}$ the auger limited lifetime can be seen. At injection levels closer to the background dopant density, the shallower transient is measured. Figure (b) displays a high injection level transient observed for a greater length of time. It is clear from the curvature of the transient that the auger limited high injection lifetime as well as the low injection lifetime are both observed. The dashed line in figure (b) shows the carrier concentration at which recombination effects switch from high injection level auger dominated recombination to low injection level SRH dominated recombination [8].

3.3 conclusions

Non-contact optical techniques represent an effective method of semiconductor characterization – particularly in the determination of minority carrier lifetime – that avoid the degradation caused by attaching electrical contacts to a sample. From a manufacturing standpoint, these benefits of these techniques are clear. Semiconductor based devices may be inspected for signs of degradation at any point along the production line, granting the ability to pinpoint precisely which production step is responsible. Additionally, the rigid spatial constraints of traditional QSSPC and MW-PCD apparatuses are avoided. The pump and probe laser need not be a specific distance from the sample, and there is a great deal of flexibility in the placement of the remaining necessary components of the pump-probe experiment.

4. Experiment

4.1 Overview

An experiment has been designed and implemented to characterize the effective minority carrier lifetime in crystalline silicon (C-Si).

At the heart of this experiment is free carrier absorption (FCA). The bandgap for C-Si is 1.12 eV. That is, the minimum required energy for an electron from the valence band to become excited to the conduction band is 1.12 eV. In this experiment electrons from the valence band are excited optically to the conduction band. To ensure sufficient photon energy to excite across the band gap a laser of wavelength shorter than 1100 nm is required. We have employed a tunable Titanium Sapphire laser which ranges between wavelengths of 720-980 nm, all of which have sufficient photon energies to produce electron-hole pairs in C-Si.

As described in section 2.2, electron-hole pairs will recombine through either SRH, radiative, or Auger recombination. Thus, an electron in the conduction band—a free carrier – will only remain there for a finite time. The lifetime of a population of free carriers is defined as the average time for which they exist in the conduction band before succumbing to one of these recombination mechanisms. However, recombination mechanisms in the bulk are problematic to isolate from surface recombination effects without undergoing surface passivation of the sample**,** and therefore we seek to determine the effective free carrier lifetime, τ_{eff}, which is a function of both the bulk lifetime and surface recombination velocity (SRV) [20].

A pump laser of wavelength $\lambda < 1100nm$, or photon energy $E_\gamma > 1.12\ eV$ is then modulated via an electro- optic modulator across a frequency range of 100 Hz to 100 kHz. Typically, we select a pump wavelength of $\lambda_{pump} = 980nm$ to allow for more uniform absorption throughout the bulk. Periodically, the photons of the pump laser are absorbed by the C-Si sample, exciting them across the bandgap from the valence band in to the conduction band. These electrons will occupy the conduction band, on average, for a time equal to the effective carrier lifetime, τ_{eff}, before recombination with a hole.

The free carriers in the material may be detected by a "probe" laser of wavelength greater than 1100nm. A laser of wavelength $\lambda_{probe} = 1550nm$, well below the bandgap energy, has been selected. In the absence of free carriers, the pump laser will pass through the material unimpeded.

Once a population of electrons has been excited to the conduction band, however, the photon energy of a 1550nm laser is sufficient to interact with these free carriers, absorbing the photon in the process [1]. The probe laser then allows us to perform a measurement of the periodic change in density of the population of electrons which have been excited to the conduction band by the pump laser. This is done by monitoring the probe laser on a detector. With the C-Si sample placed between the probe laser and the detector, in the absence of the pump laser, a constant DC signal will be detected. When the pump laser is allowed to strike the sample, the resulting population of free carriers in

the conduction band will attenuate the probe laser resulting in a decrease of the measured DC signal.

This experiment differs in a major way from steady state and quasi-steady state measurements of FCA. Rather than building to a quasi-steady state, the pump laser being modulated by an electro-optic modulator at a set frequency creates a periodic pulse of photons which creates a population of free carriers in the conduction band at the same frequency as the modulation of the pump beam. The probe beam is attenuated at the same frequency as the probe beam. The output from the detector is then fed in to a lock in amplifier which is referenced to the frequency of the pump beam's modulation. In doing so, the periodic attenuation of the probe beam can be detected by the lock in amplifier. This method alone does not contain sufficient information to determine τ_{eff}, however, by performing the above measurement across a range of frequencies, the necessary information may be gathered, as detailed below.

At low frequencies, f , such that $\frac{1}{f} > \tau_{eff}$, the population of electrons excited in to the conduction band will have sufficient time to recombine entirely between pulses from the pump laser. This will result in the maximum amplitude of periodic attenuation in the probe beam, as the detector will measure both the full intensity of the probe beam as well as the lower intensity due to attenuation, resulting in an amplitude $A_{small\ f} = I_{full} - I_{attentuated}$. At frequencies sufficiently large that $\frac{1}{f} < \tau_{eff}$, there will not be sufficient time for the entire population of electrons in the conduction band to recombine before the next pulse of the pump beam arrives and excites a new population. Consequently, the amplitude of the periodic attenuation of the probe beam at higher frequencies will be smaller than $A_{small\ f}$, since the intensity of the probe beam will never be able to recover to I_{full} . When the amplitude of attenuation of the probe beam is plotted against frequency of modulation of the pump beam, a lorenztian curve results. This curve may be fit to what is essentially a first order low pass filter (see section 2.3.3) in order to determine the characteristic time scale which is, uniquely, τ_{eff}.

4.2 Procedure

A 1550nm probe laser is incident on a C-Si sample placed in a sample holder as in figure 4.1. The probe laser radiation which passes through the sample is collected on an infrared detector which measures incident power.

A variable wavelength pump laser, of wavelengths $720nm < \lambda < 980nm$, first passes through an electro-optic modulator before illuminating the sample as well. The probe beam is expanded by means of a beam expander in order to cover the entire aperture of the sample holder and ensure that both the pump and probe beams overlap where they illuminate the sample.

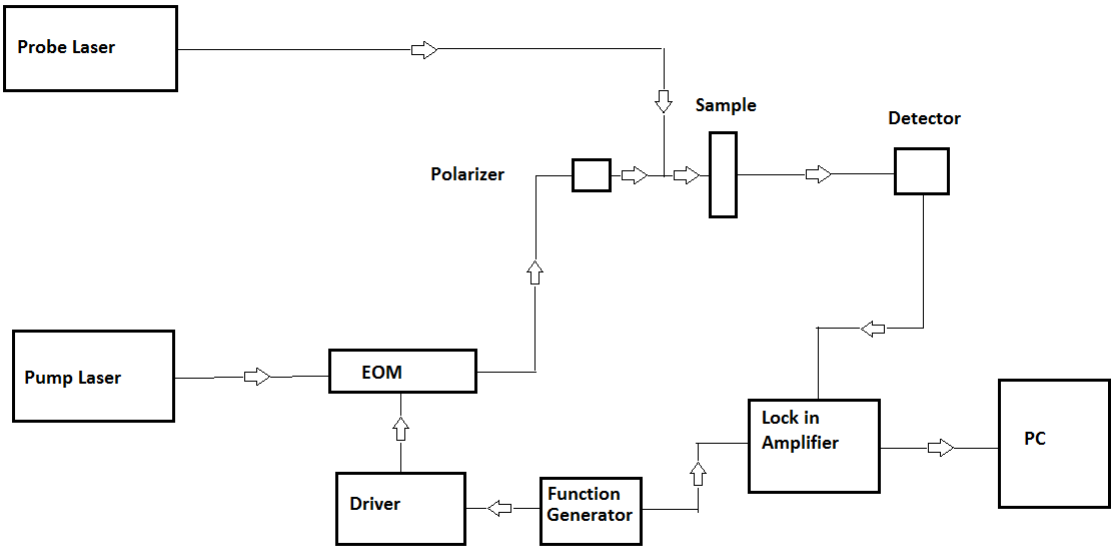

Figure 4.1: Block diagram of MFCA experiment. The pump laser passes through an electro-optic modulator before passing through an adjustable polarizer, and striking the sample. A 1064 nm long pass filter is used at the detector to attenuate any light from the pump laser that survived the sample. The probe laser strikes the sample at the same location as the pump. The detector measures the drop in intensity of the probe laser due to MFCA and sends this signal to the lock in amplifier to be compared against a sinewave at frequency f that the function generator sends the both the EOM driver and the lock in amplifier. Finally, the lock in amplifier writes data to a PC for analysis.

A function generator feeds a sine wave signal of a frequency f to a driver for the modulator which in turn causes the pump laser to be modulated at frequency f. The signal of the detector measuring the probe laser is input to a lock in amplifier synced with the frequency output by the function generator. By plotting the change in intensity of the probe laser measured at each frequency against frequency and fitting the data to equation 5.1, the time constant describing the effective minority carrier lifetime, τ_{eff}, may be extracted from the data.

4.3 With Respect to Injection Level

As described in 2.1, injection level is defined as the average density of excess minority carriers due to absorption of photons of energy greater than the band gap.

Injection level in this experiment is controlled by two parameters: a variable half wave plate polarizer and a lens. The polarizer is set in the path of the pump beam to allow control over the intensity of light which passes to the sample. By decreasing the intensity, the number of photons incident on the sample is decreased proportionally resulting in a lower injection level. Conversely, the injection level may be raised by focusing the pump beam with a lens, reducing the area of illumination on the sample.

The distance of the lens to the sample allows control over the area of the pump beam spot as it strikes the sample. If the lens is at a distance equal to its focal length, the pump beam spot will experience maximum contraction, and thus cause the maximum increase in injection level at a given intensity. As the lens is moved further from the sample, the area of the pump beam spot on the sample expands, and the injection level will decrease.

In the case of a sample having spatial variability in lifetime, care must be taken to ensure the pump beam is centered on the same location of the sample for each measurement, and that the spatial variation be large compared to the pump beam. A track has been constructed which allows the lens to be moved towards or away from the

sample while remaining centered on the trajectory of the pump beam. In this way the spot size of the pump beam may be controlled while remaining centered on the same area of the sample at each position.

4.4 Reflection mode

Importantly, the sample is mounted on a rotating stand, allowing control of the angle of incidence of both the probe and pump beams. By constraining the probe beam to strike the sample at an angle normal to the sample plane, the reflected part of the probe beam may be collected on a second, identical, detector.

A lens is placed near the sample in order to collect diffuse scattered reflected light from the probe beam in the case of textured samples, and focus the light on to the detector to improve signal strength.

5. Methods of Data Analysis

Scripts have been written in order to automate the process of data acquisition. First, both the amplitude and phase output from the lock in amplifier – as described in section 4 above – are output to a CSV file along with the frequency at which each measurement was taken. The amplitude data is then written to arrays and sorted by frequency. If multiple data at a single frequency were taken, amplitude values are averaged before the mean value is placed in to an array.

Once sorted, the amplitude data is plotted against frequency. To aid in visualization, the frequency axis is logarithmic. A typical result is shown below in figure 5.1.

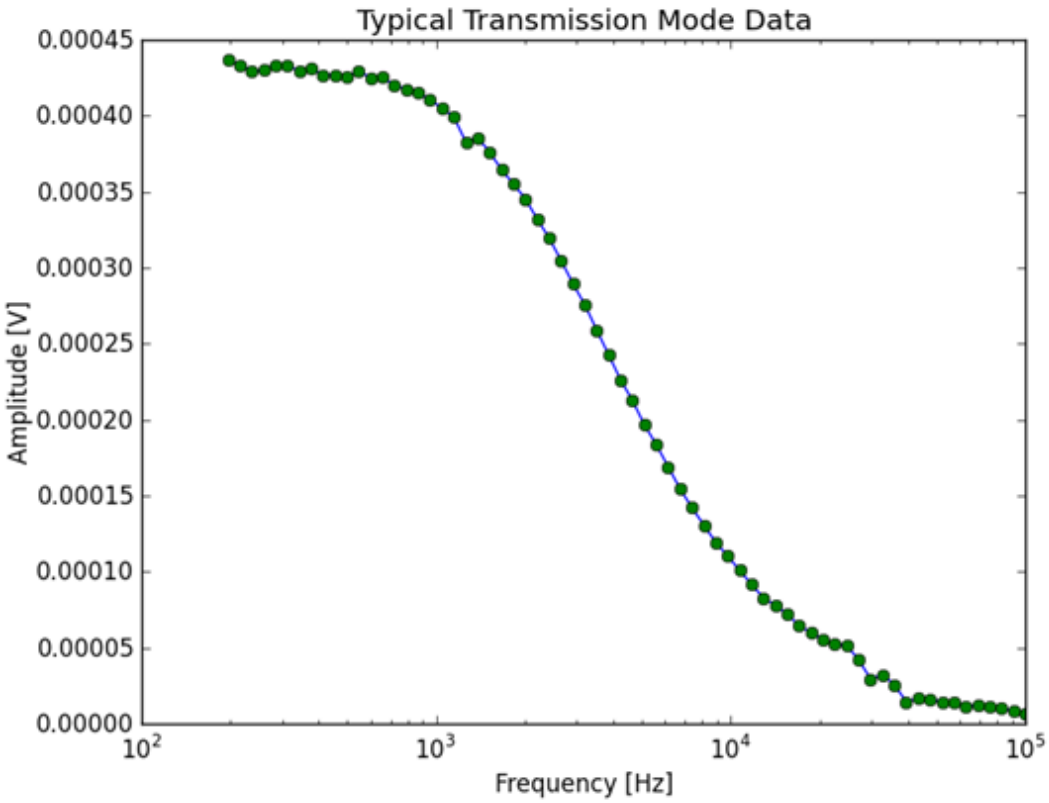

Figure 5.1: Typical example of the Lorentzian roll off output by the pump-probe MFCA experiment.

5.1 Signal Strength and Background

The data presented in figure 5.1, with the exception of some averaging, is simply the raw output of the lock in amplifier at each frequency. In general, one should consider the contribution from the probe beam, the pump beam, and the background noise present in the experiment. Each of these may be isolated by running the experiment with the pump beam shutter closed in order to measure only the contribution of the probe beam, the probe beam shutter closed to measure only the contribution of the pump beam, and both the pump and probe shutters closed so as to measure the background noise in the experiment. Comparisons of the probe, pump, and background noise to the signal in

transmission mode will be shown throughout this section. We note, in the exception of measuring diffuse scattered light, that similar ratios are present in reflection mode.

In the case of the work presented in this thesis, the contribution from the pump and probe lasers, as well as the noise inherent in the experimental apparatus are much weaker than the detected signal. It should be noted that the detector frequency response is not flat, as seen in figure 5.2, and must be accounted for when analyzing data in order to avoid artificially high amplitudes. This may be accomplished by dividing the output data array by the frequency response array measured across the same frequency range.

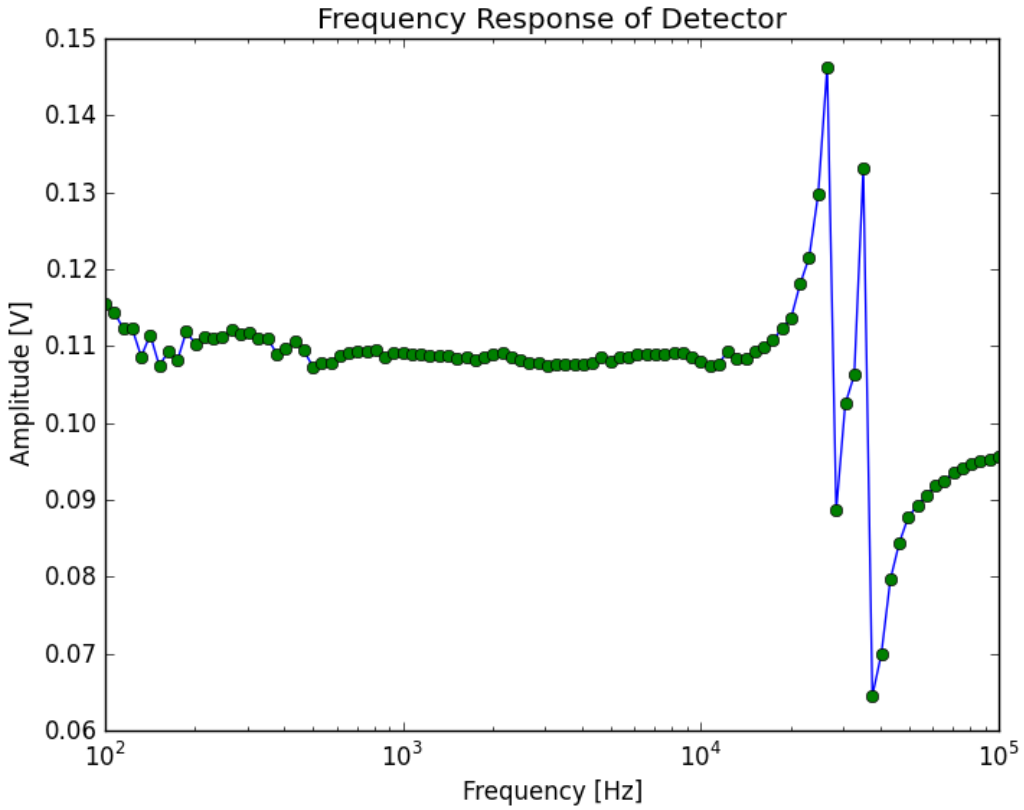

Figure 5.2: Frequency response for IR photo receiver detector

Let us first consider the contribution of the probe laser, as seen in figure 5.3. In the case presented in this section – which is representative of the output of this experiment excepting measurements of diffuse scattered reflection as outlined in section 6.3 – the mean value of the probe laser amplitude across the entire frequency range measured is $Probe_{mean} = 3.74x10^{-6}\ V$, whereas the mean value of the signal in Transmission mode is $Trans_{mean} = 2.25x10^{-4}\ V$, approximately sixty times greater than $Probe_{mean}$.

We note that the minimum Signal output from the Transmission mode data is $Trans_{min} = 6.44x10^{-6}\ V$ while the maximum value reached by the probe laser is $Probe_{max} = 1.41x10^{-5}V$. From figure 5.3, however, it is noted that the frequency range where the amplitude of the probe laser signal takes its greatest values is also the frequency range where the output amplitude signal of the experiment takes its greatest values, and that they exceed the amplitude of the probe beam in this region by greater than an order of magnitude.

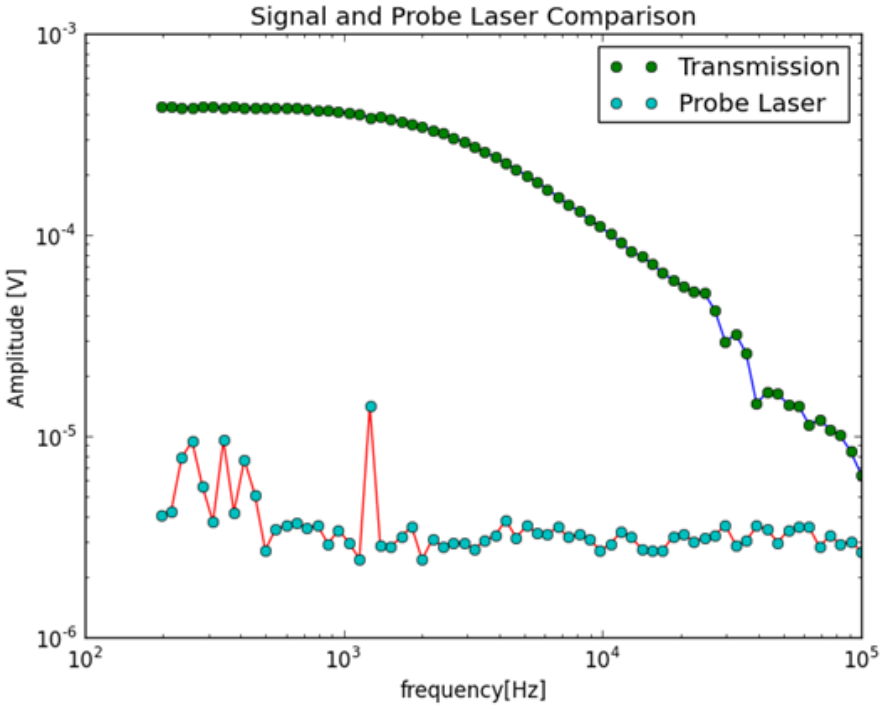

Figure 5.3: comparison between the Transmission mode data and contribution of the probe laser.

Let us now consider the contribution of the Pump laser, as seen in figure 5.4 below. The mean amplitude of the pump laser signal is $Pump_{mean} = 2.05x10^{-6}\ V$, approximately 110 times weaker than the mean output signal of the experiment in transmission mode.

As can be seen from figure 5.4, the amplitude of the pump beam signal is always less than the output signal of the experiment across the entire frequency range.

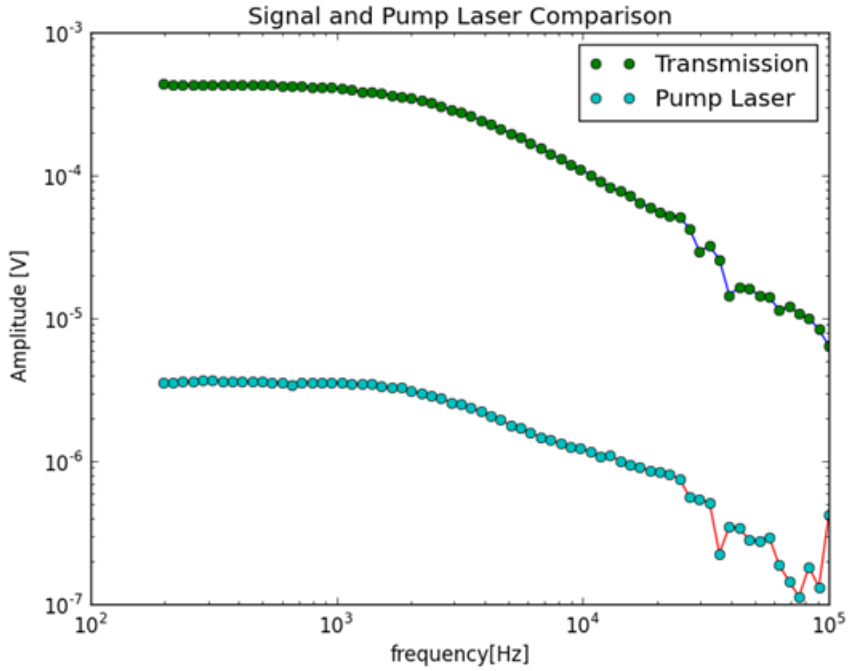

Figure 5.4: Comparison of the Transmission mode data and the contribution from the pump laser.

Finally, the mean value of the background across the entire frequency range is $Background_{mean} = 4.35x10^{-7}\ V$, approximately 520 times smaller than $Trans_{mean}$. It can be seen from figure 5.5 that the background is negligible compared to the output signal of the experiment. Ratios of the output signal to the probe, pump, and background can be seen below in figure 5.6.

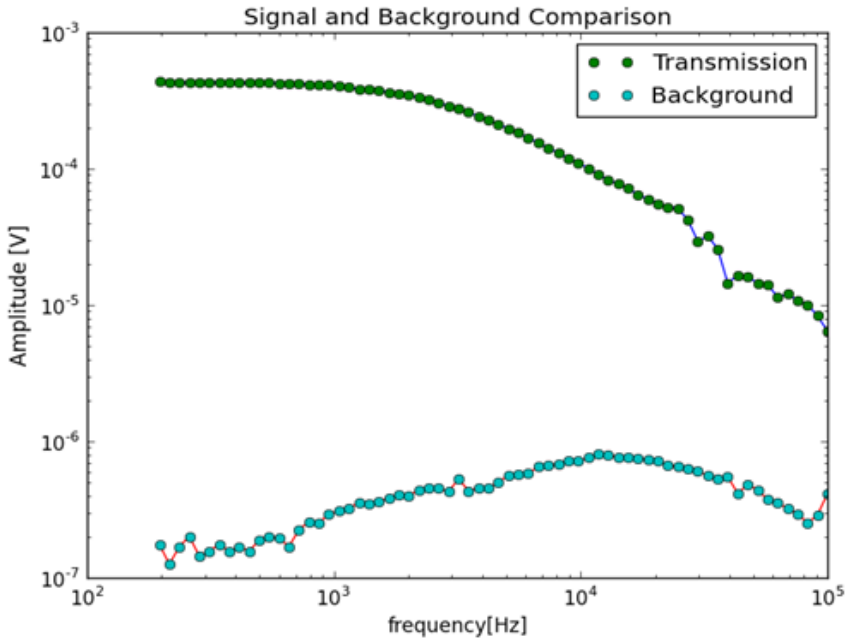

Figure 5.5: Comparison of Transmission mode data and the contribution from noise. Pump and probe both blocked..

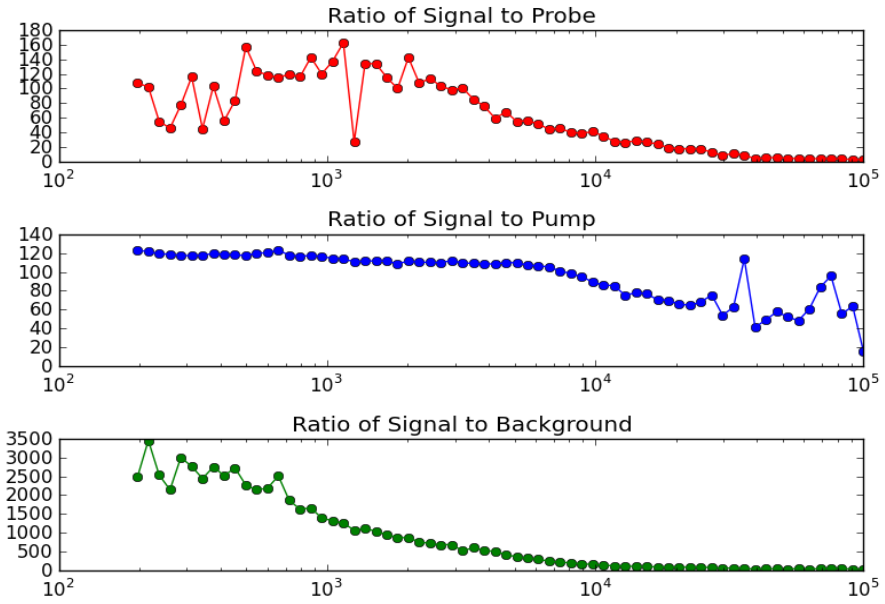

Figure 5.6: ratios between the transmission amplitude and the probe, pump, and background amplitudes respectively.

As the contribution from the probe beam, pump beam, and background amplitudes are sufficiently low compared to the amplitude of the output signal of the experiment as to be negligible, these data are typically not recorded and subtracted from the output of the experiment as to maximize speed of acquisition -- a particularly useful trade off when considering the use of this in an in line manufacturing process. The exception being if the signal from the experiment is very low, as in the case of measuring the diffuse reflection of a textured sample, as in section 6.3.3.

5.2 Effective Lifetime Determination

Once the data is collected, the effective lifetime τ_{eff} must be determined. The data can be fit to a lorentzian roll off modelled by the following:

$$C\frac{1}{\sqrt{1+\left(2\pi f\tau_{eff}\right)^2}}, \tag{5.1}$$

where f is the frequency τ_{eff} is the effective lifetime and C is a constant which scales the amplitude of the Lorentzian – as the amplitude at each frequency is $\ll 1$ – The SR830 lock in amplifier allows a maximum input of 1V – this constant is necessary in order to allow for an accurate fit. The parameters C and τ_{eff} are determined by a least squares fit of the data performed using the Python library Lmfit. The output of this fit for the data discussed above can be seen in figure 5.7. The lifetime is determined to be $\tau_{eff} = 61.8\ \mu s$ and the scaling parameter is determined to be $C = 4.35x10^{-4}\ V$.

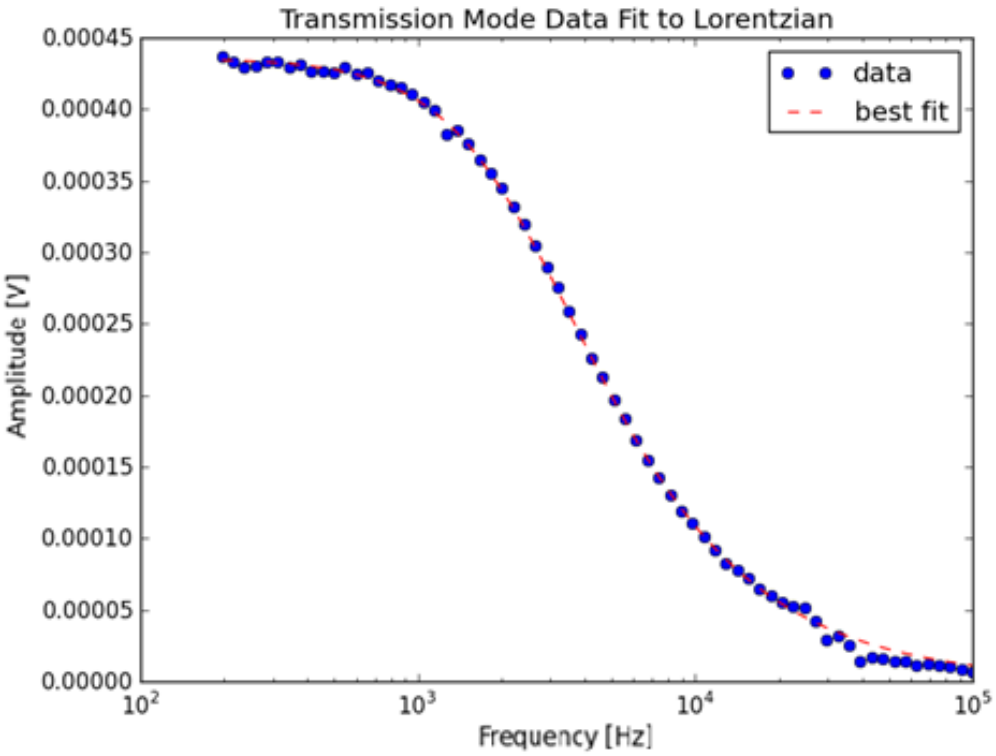

Figure 5.7: output data from the pump probe experiment, fit to the lorentzian curve described in equation 5.1. the calculated effective lifetime is $tau_{eff} = 61.8\ \mu s$.

5.3 Calculating Injection Level

As in section 2.2, we define the injection level as the average density of minority carriers present in the material. In order to determine this value the generation rate, G, of minority carriers must first be calculated.

The diameter of the pump beam is first measured with a beam profiler allowing for the area of the beam spot to be determined. As the angle at which the pump beam strikes the sample is off-incident, the area illuminated by the pump will be elliptical in shape. This must be accounted for in order to accurately determine the density of minority carriers.

With the surfaces sufficiently polished, the pump beam can be assumed to move in an elliptical column through the sample. The generated carriers must then be contained in a volume

$$V = ab\pi^2 \cdot d\ , \tag{5.2}$$

where a and b are the radii of the ellipse and d is the length of the column,

$$d = \frac{W}{\cos(\theta)}, \tag{5.3}$$

where W and θ are, respectively, the thickness of the sample and angle the probe beam makes with the normal to the sample.

A photon of wavelength λ has an energy of

$$E_\lambda = \frac{hc}{\lambda}\,, \tag{5.4}$$

where h is Planck's constant and c is the speed of light.

The power absorbed by the sample is determined by measuring the power of the pump beam before it reaches the sample, and the reflected and transmitted intensities. These measurements are performed with a Gentec-EO power meter. By subtracting the measured reflected and transmitted intensities from the initial intensity of the pump beam the fraction of the power absorbed in the sample is determined:

$$P_{absorbed} = P_{incident} - P_{reflected} - P_{transmitted} \tag{5.5}$$

The number of photons absorbed per second in the material can be found by taking the ratio of the power absorbed to photon energy:

$$G = \frac{P_{absorbed}}{E_\lambda} \quad . \tag{5.6}$$

Assuming that every photon absorbed created an electron-hole pair, G is equal to rate of generation of minority carriers in the conduction band.

Once an effective lifetime has been determined by the method described in section 5.2, the injection level may be calculated as:

$$\Delta n = G\tau_{eff} \quad . \tag{5.7}$$

It should be noted that $P_{incident}$ is a function of time, as the pump laser is fed through an electro-optic modulator (EOM). The EOM is driven by a function generator sending a sine wave at frequency f, thus $P_{incident}$ is sinusoidal as well.

In determining the injection level we are concerned with the peak to peak AC amplitude of $P_{incident}$. The modulated pump beam, $P_{incident}$,is measured on a Newport model 2033 large area IR photo receiver and viewed on an oscilloscope. The peak to peak voltage and average voltage of the measured sine wave are recorded.

The Gentec power meter has a sufficiently slow response time that the measured power of the modulated pump beam will be the average of the peak to peak AC power. The AC/DC voltage ratio measured with the IR detector and the AC/DC power ratio are equivalent. From the measured DC power on the Gentec-EO power meter, we may then infer the peak to peak AC power of $P_{incident}$.

As a final caution, consider that the function generator is first passed through a driver for the EOM. The driver allows for a DC bias to be manually set, and doing so will affect the ACV/DCV ratio. If the DC bias on the driver is changed, the ratio will need to be recalculated.

6. Experimental results

6.1 Transmission Mode

We define transmission mode as monitoring the intensity of the part of the probe beam which is transmitted through the sample. As can be seen in figure 6.1 the probe beam is aligned with the detector, and perpendicular to the plane of the sample. This geometry maximizes the intensity incident on the detector to ensure a strong signal to noise ratio.

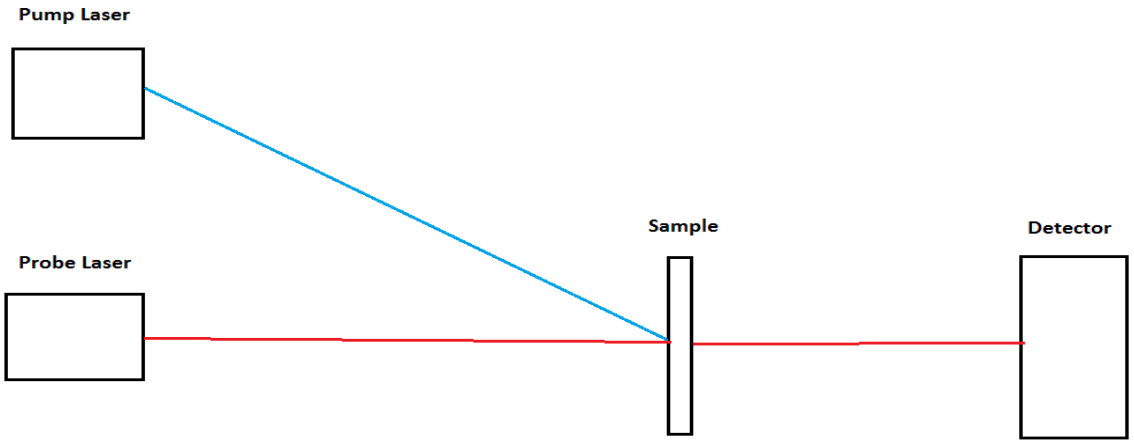

Figure 6.1: Transmission mode geometry. The pump laser and probe laser strike the sample at the same point, with a detector placed behind the sample to collect the transmitted probe beam.

Below we present transmission mode data for four silicon samples: Two intrinsic <100> float zone silicon samples, an N-type Si:P , <100>, Czochralski grown silicon sample, and an N-type Si:P ,<100> float zone sample. Both intrinsic samples are taken from the same wafer, with one subject to silicon nitride deposition and the other left un-passivated.

The data presented below demonstrates the ability of this experiment to measure the effective lifetime across a range of silicon samples.

6.1.1: Pasivated Intrinsic Silicon

The data presented in figure 6.2 is for a sample of crystalline float zone silicon of orientation <100> that has been subjected to silicon nitride deposition at McMaster University. This is in order to soak up dangling bonds which may be present at the surface, and to better probe the bulk lifetime of the sample.

The sample has a resistivity stated by the manufacturer to be $> 3000\ \Omega \cdot cm$, and a thickness of $575\ \mu m$.

A pump wavelength of $\lambda_{pump} = 970\ nm$ at an injection level of $\Delta n = 2.1x10^{16}\ cm^{-3}$ has been used to excite free carriers across the bandgap, and a probe laser of wavelength $\lambda_{probe} = 1550\ nm$ has been used to measure the modulated free carrier absorption (MFCA).

Fitting the data presented in figure 6.2 to equation 5.1, an effective lifetime of $\tau_{eff} = 47.0\ \mu s$ is measured at this injection level.

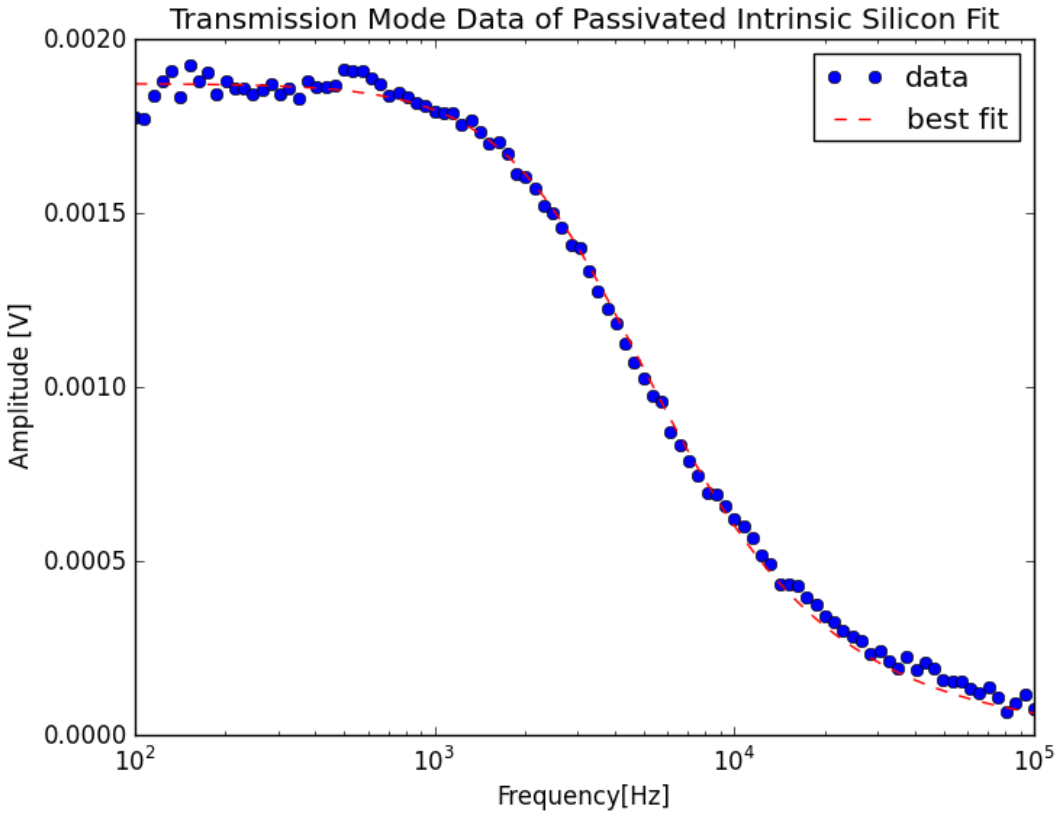

Figure 6.2: Transmission mode data is shown for a 575μm thick sample of float zone <100> silicon of resistivity > 3000 ohm-cm. The surface of the sample has been passivated by silicon nitride deposition. The data has been fit to equation 5.1 for a calculated effective lifetime of $\tau_{eff} = 47.0\ \mu s$, at an injection level of $\Delta n = 2.1x10^{16} cm^{-3}$.

6.1.2: Intrinsic (Un-passivated) Silicon

This sample is from the same wafer as the sample in section 6.1.1, the only distinction being that this sample has not been subject to passivation. At a thickness of 575 μm one should expect that the lifetime will be limited by surface recombination, decreasing the minority carrier lifetime when compared against its passivated counterpart.

The passivated an un-passivated samples were measured under the same conditions on the same day. The incident angles of the pump and probe beams, the

incident power of the pump, and thus the generation rate, were the same between samples and the measurement of the un-passivated sample was made immediately after the measurement of its passivated counterpart to ensure the most direct comparison.

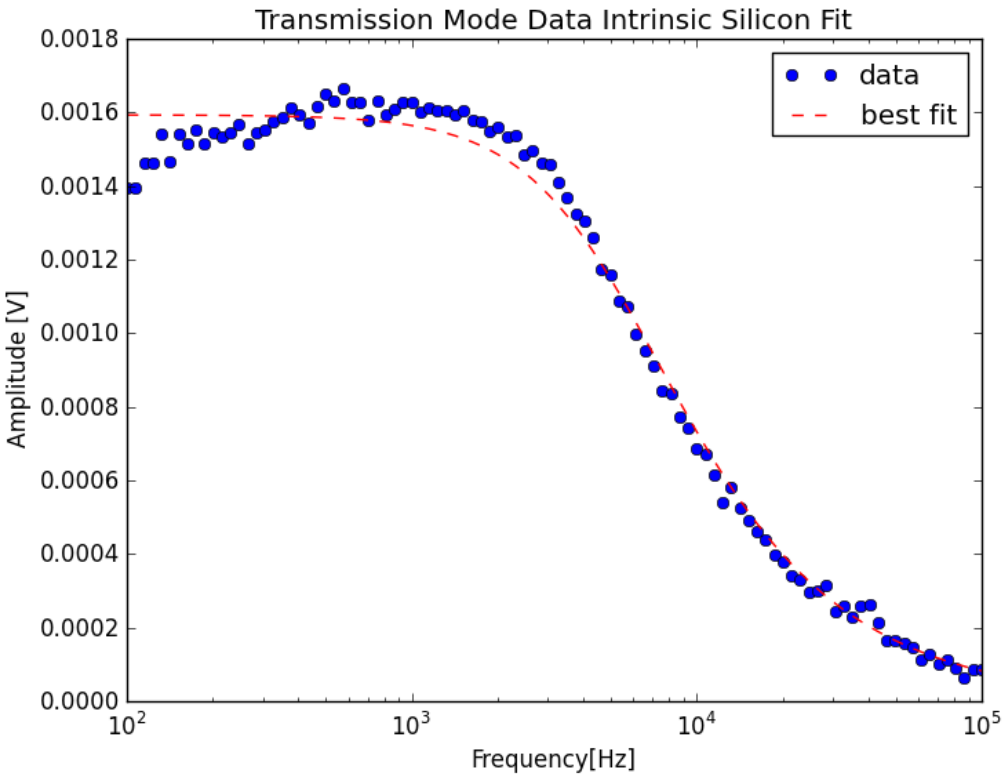

Figure 6.3: Transmission mode data is shown for a 575μm thick sample of float zone <100> silicon of resistivity > 3000 ohm-cm. The data in both this plot and that of figure 6.2 are taken from two samples of the same wafer, however the surface of this sample was not subject to passivation. The effective lifetime is determined to be $\tau_{eff} = 30.7\ \mu s$ at an injection level of $\Delta n = 1.3x10^{16} cm^{-3}$.

Figure 6.3 displays the data of the un-passivated intrinsic sample fit to equation 5.1. An effective lifetime of $\tau_{effective} = 30.7\ \mu s$ is determined for this sample. This effective lifetime is shorter than what was measured on the passivated sample – $\tau_{effective} = 47.0\ \mu s$ – and this is likely due to the surface passivation decreasing the SRV and increasing the effective lifetime. In drawing this comparison, however, some caution is required. The lifetime across the surface of the passivated sample is non-

uniform, suggesting that surface passivation is imperfect[1]. Though a distinct difference in measured effective lifetime is seen between the passivated and non-passivated samples, in neither case is the bulk lifetime being measured independently of the SRV.

6.1.3: N-type Un-passivated Silicon

Figure 6.4 displays the experimental results and fit for an un-oxidized, N-type, Si:P, Czochralski grown crystalline silicon of <100> orientation. The resistivity is $1 - 20\ \Omega \cdot cm$ as quoted by the manufacturer, and the thickness is 1.5 mm.

As was the case for the previous two samples, the pump light wavelength is $\lambda_{pump} = 970nm$ and the probe light wavelength is $\lambda_{probe} = 1550\ nm$.

The manufacturer has polished only one side of the wafer, however, in order to prevent light from the probe beam scattering off the rear surface of the sample, the rear surface was polished on premises at McMaster University. By preventing the scattering of probe light upon exiting the sample, the probe may be more efficiently coupled in to the detector.

At an injection level of $\Delta n = 1.3x10^{16}\ cm^{-3}$, the effective minority lifetime of the sample was measured to be $\tau_{eff} = 111.1\ \mu s$.

[1] See section 7.1.

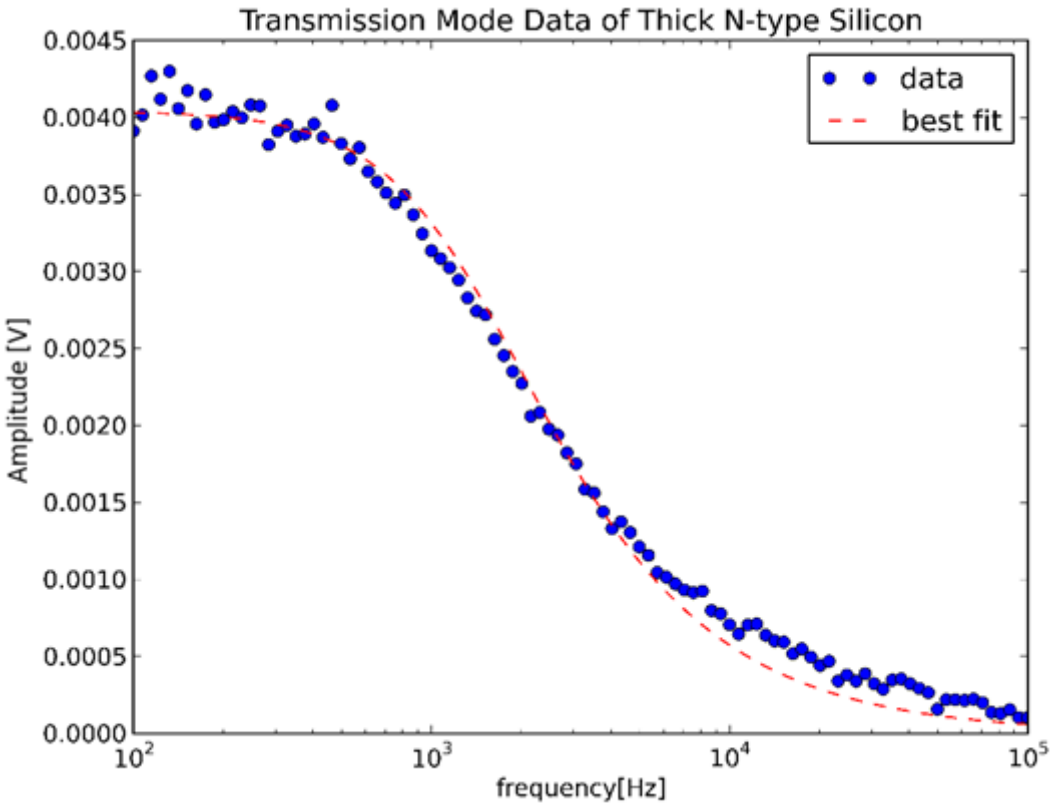

Figure 6.4: Lorentzian fit of transmission mode data is shown for 1550 μm thick Czochralski grown <100> silicon of 1-20 ohm-cm resistivity. The sample is N-type (dopant: Phosphorus) and un-oxidized. Wafers arrived from manufacturer with one side polished. The second side was polished on premises at McMaster University. The data has been fit to determine an effective lifetime of $\tau_{eff} = 111.1\ \mu s$ at an injection level of $\Delta n = 1.3x10^{16} cm^{-3}$.

Figure 6.5 shows the experimental output and lorentzian fit for a sample of N-type (phosphorus doped) 300 μm thick sample of float zone grown <100> silicon. The manufacturer has polished both sides of the wafer with a quoted resistivity of $1 - 5\ \Omega$cm.

The effective lifetime is determined to be $\tau_{effective} = 54.5\ \mu s$ at an injection level of $\Delta n = 4.1x10^{16} cm^{-3}$.

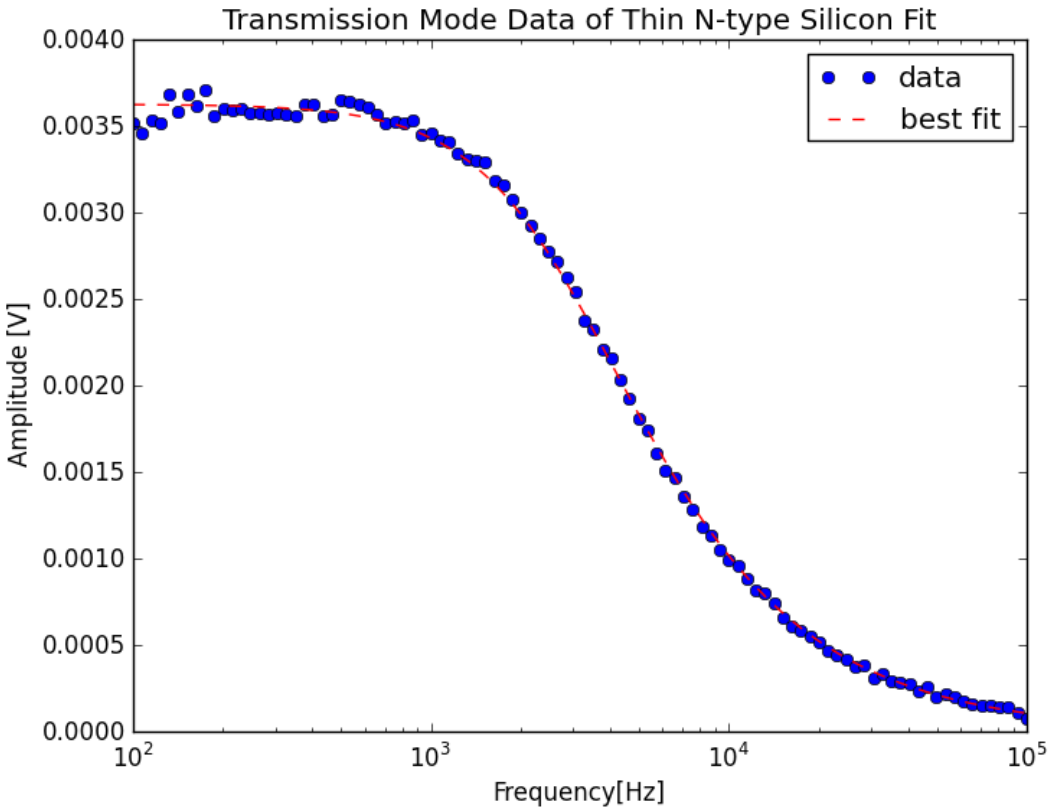

Figure 6.5: Lorentzian fit of transmission data is shown for a 300 μm thick, float zone, N-type Si:P, <100> Silicon sample. The pump beam wavelength is $\lambda_{pump} = 980\ nm$ and the probe beam wavelength is $\lambda_{probe} = 1550\ nm$. At an injection level of $\Delta n = 4.1x10^{16} cm^{-3}$ the effective lifetime is calculated to be $\tau_{effective} = 54.5\ \mu s$.

Sample	**Injection level $[cm^{-3}]$**	**Effective Lifetime $[\mu s]$**
Intrinsic Passivated	$\mathbf{2.1x10^{16}}$	**47.0**
Intrinsic	$\mathbf{1.3x10^{16}}$	**30.7**
N-type (1.5 mm)	$\mathbf{1.3x10^{16}}$	**111.1**
N-type (300 μm)	$\mathbf{4.1x10^{16}}$	**54.5**

Table 6.1: injection level and measured lifetime of samples discussed in this section.

6.2: Injection level Dependence

The injection level dependence of the effective lifetime is investigated for two samples. The passivated, intrinsic, FZ silicon sample, and the thick, N-type, CZ silicon sample. A pump wavelength of $\lambda_{pump} = 980\ nm$ is used, and a probe wavelength of $\lambda_{probe} = 1550nm$. In order to ensure an overlap of the pump and probe lasers when increasing and decreasing the area of the pump, the probe beam is passed through a beam expander such that it illuminates the entirety of the sample. It may be necessary to increase the power of the probe beam while employing the beam expander in order to maintain sufficient signal strength.

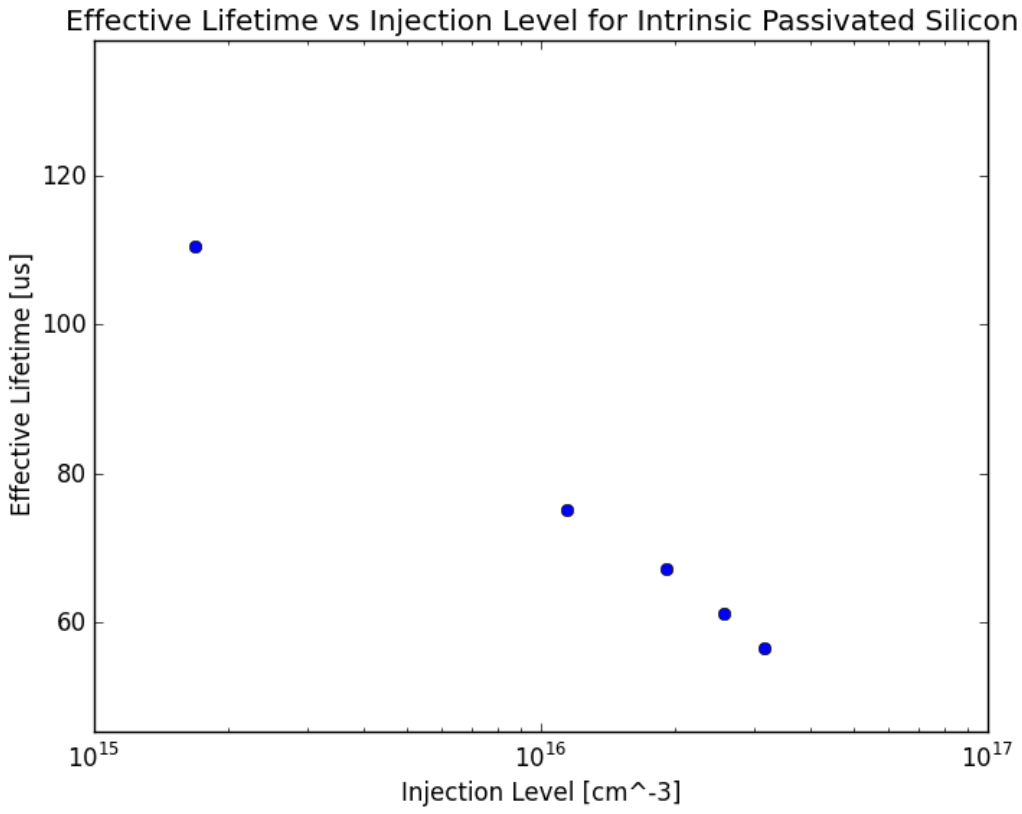

Figure 6.6: Injection level vs effective lifetime for the passivated 575μm thick sample of float zone <100> silicon of resistivity > 3000 ohm-cm. Effective lifetime of the sample can be seen to increase as the injection level is decreased.

The case of the intrinsic silicon sample is interesting. A clear increase in measured effective lifetime is seen in figure 6.6 as the injection level is decreased. As discussed in section 2.2 it is to be expected that as the injection level is further decreased the trend should reach an inflection point, and the measured effective lifetime should begin to decrease. However, difficulty arose in attempts to perform lifetime measurements at lower injection levels due to the spatial variations in the lifetime of the sample[2]. This non-uniformity of the sample's lifetime is problematic for probing across a large range of injection levels, as expanding or contracting the area of the probe beam introduces a large uncertainty in measurement.

In attempting to measure at lower injection levels, the area of the pump beam is expanded, increasing the likelihood that multiple regions of effective lifetime occupying the same area excited by the pump. For this reason, the area of pump beam was held constant and the injection level was altered via only attenuation by the polarizer. This constraint limited the range of injection levels considerably.

The un-passivated intrinsic sample has a much higher spatial uniformity in lifetime than the passivated sample, making it the superior candidate for measurement of injection level dependence by this method, however, injection level dependence of the non-passivated sample was not detected in the author's experiments.

The thick, N-type sample is a more appropriate candidate for investigating the injection level dependence of effective lifetime for the MFCA pump-probe experiment. At 1.5 mm thick, any lifetime degrading effects attributable to the surface will be minimized. As well, the pump wavelength of $\lambda_{pump} = 980\ nm$ will provide uniform generation of carriers throughout the relatively large bulk of the sample. Like the non-passivated intrinsic sample, this sample has a good degree of spatial uniformity in effective lifetime, and thus one may expect to avoid the problems discussed above. Measurements of effective lifetime across a range of injection levels for this sample are shown in figure 6.7.

[2] Refer to section 7.1 for further information on the spatial uniformity of this sample as well as others discussed in this section.

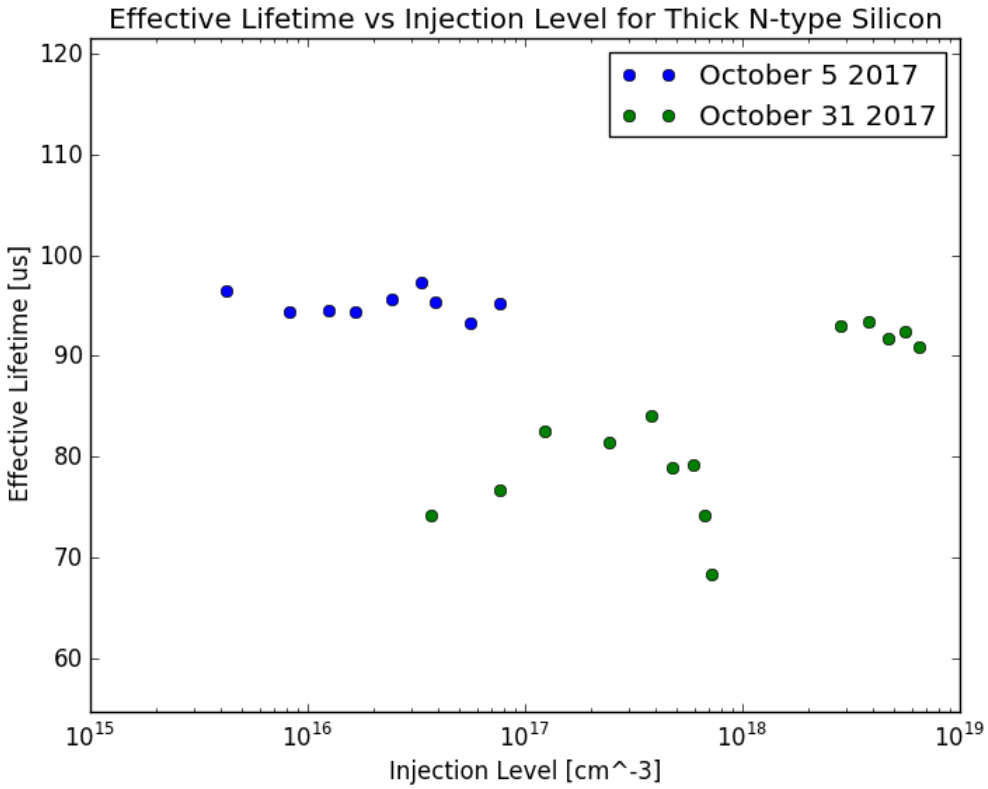

Figure 6.7: Injection level vs effective lifetime measurements for 1550 μm thick Czochralski grown <100> silicon of 1-20 $\Omega - cm$ resistivity. Measurements shown in blue were taken on October 5 2017 and measurements shown in green were taken on October 31 2017. The October 5 measurements do not appear to show an injection level dependence on effective lifetime, nor do the $> 10^{18}\ cm^{-3}$ injection level measurements from October 31.

The measurements shown in figure 6.7 were performed on two separate occasions. Those shown in blue were performed on October 5 2017, while those shown in green were performed on October 31 2017. The measurements from October 5 do not appear to show any dependence of effective lifetime on injection level across the measured range of injection levels. As discussed in section 2.2, below a critical injection level one should not expect to see a large dependence in the effective lifetime, however, measurements performed on October 31 across comparable injection levels appear to

show an increase in effective lifetime with injection level, before a steep decrease approaching an injection level of $10^{18}cm^{-3}$.

A large discrepancy in measured effective lifetimes at similar injection levels between the data from October 5 and October 31 is obvious in figure 6.7. Given the spatial uniformity of this sample, this is not likely due to measuring different locations of the sample or adjusting the area of the pump beam. The drop in effective lifetime of the sample at these injection levels is likely not due to degradation of the sample as above an injection level of $10^{18}cm^{-3}$ the effective lifetime becomes comparable to the low injection level lifetimes measured on October 5. The reason for the increase in lifetime at high injection level is not clear.

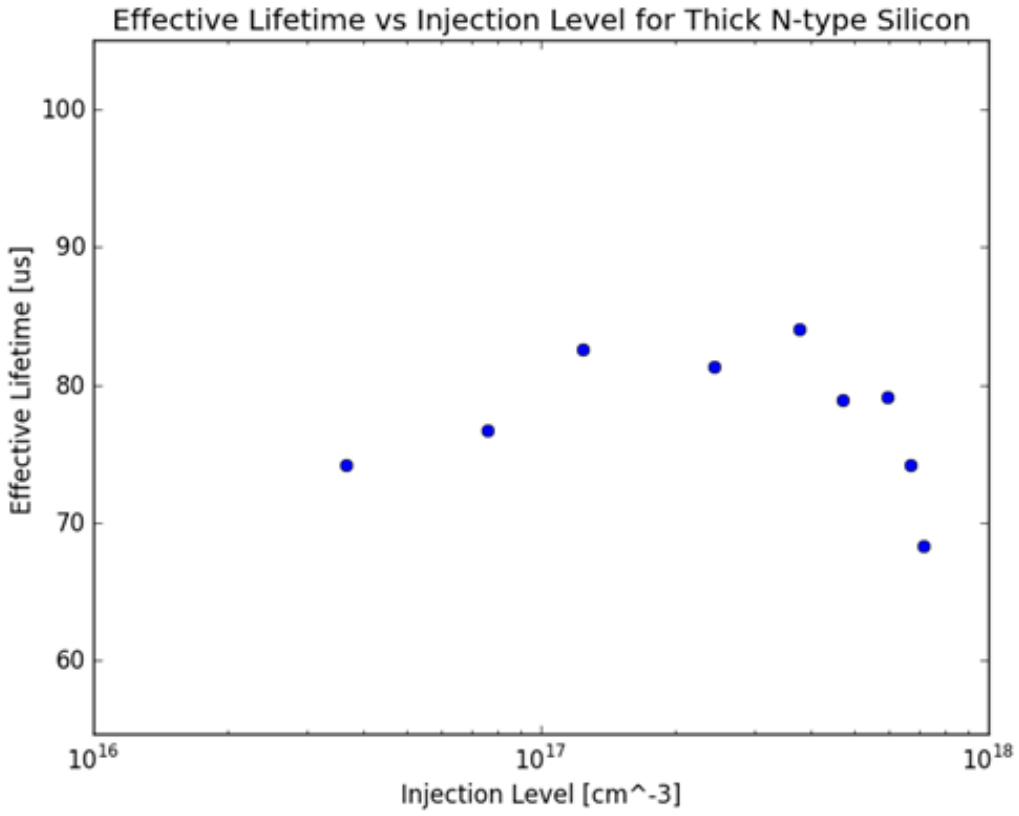

Figure 6.8: A closer look at the $< 10^{18}cm^{-3}$ October 31 measurements shown in figure 6.7.

Figure 6.8 shows only the lower lifetime measurements taken on October 31, and while there does appear to be an increase in lifetime before a steep decay, the author would caution against drawing any concrete conclusions of these measurements given the issues discussed here.

6.3 reflection mode

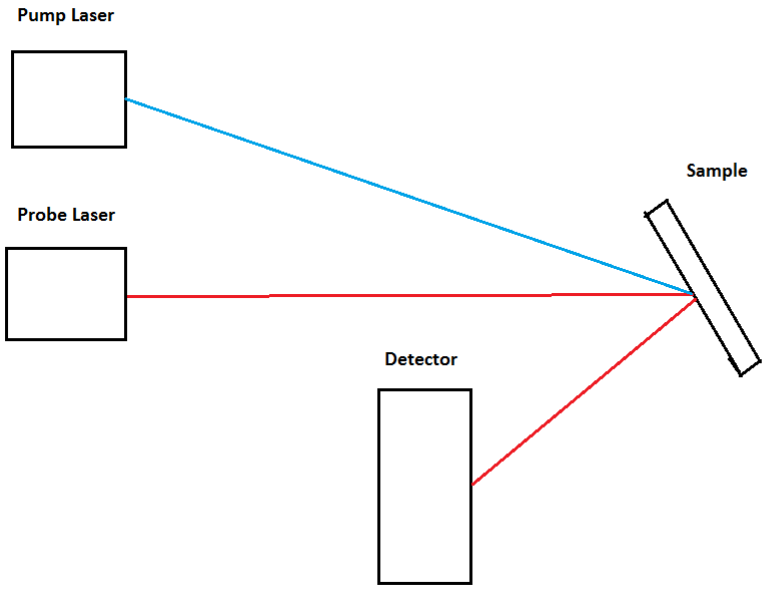

Figure 6.9: The pump and probe beams strike a sample at the same location. The sample is rotated such that the reflected part of the probe beam may be monitored on a detector.

The experimental apparatus is capable of detecting MFCA in the reflected part of the probe beam as well, by the geometry illustrated in figure 6.9. Rather than placing a detector behind the sample, as in transmission mode, the sample is rotated to allow the reflected part of the probe beam to be monitored on a detector.

The reflection mode geometry is particularly useful when performing lifetime measurements on samples with metalized backings, as no light from the probe will be permitted to transmit through the sample. This would allow for contactless in line

monitoring of lifetime during the solar cell fabrication process, beyond the point where pump probe technique are traditionally useful.

Figure 6.10 shows the output of the experiment in reflection mode for a 1.5mm thick, N-type, <100>, Czochralski grown silicon sample. The data is fit to equation 5.1, and the effective lifetime is determined to be $\tau_{eff} = 87.7\ \mu s$ for an injection level of $\Delta n = 6.3x10^{15} cm^{-3}$.

A transmission mode measurement of the same sample was shown in the previous section in which an effective lifetime of $\tau_{eff} = 111.1\ \mu s$ was measured at an injection level of $\Delta n = 1.3x10^{16}\ cm^{-3}$. In order to definitively compare lifetime measurements taken in reflection mode and transmission mode geometries, however, the measurements must be taken on the same sample, and under the same conditions.

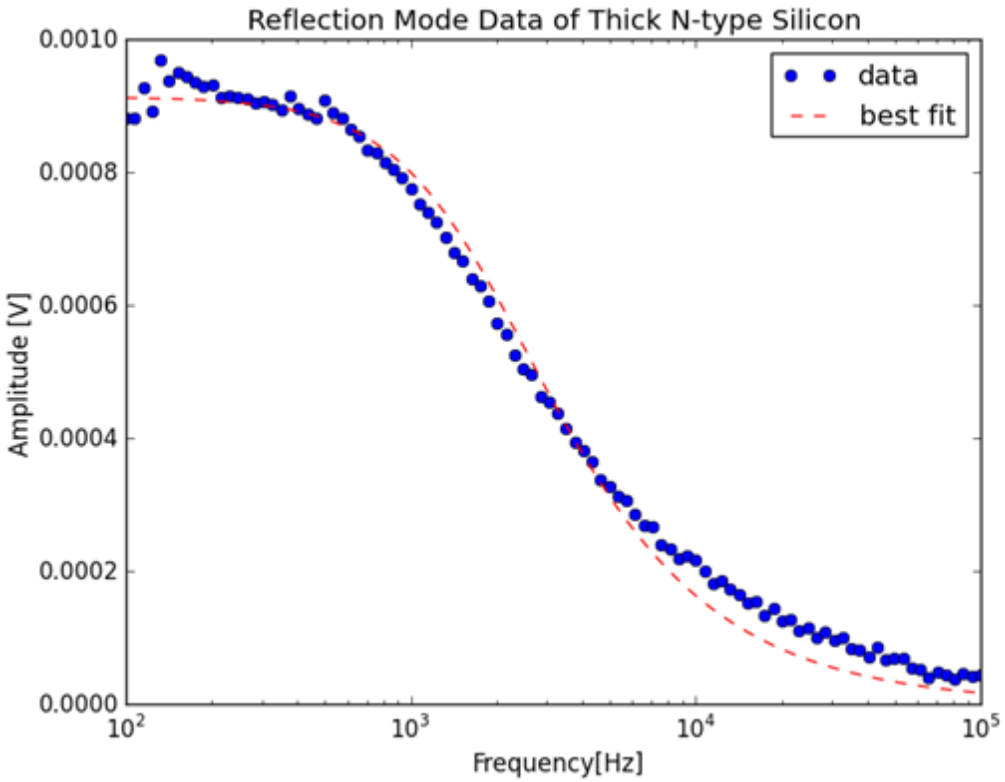

Figure 6.10: a Lorentzian fit of Reflection mode data is shown for 1550 μm thick Czochralski grown <100> silicon of 1-20 $\Omega - cm$ resistivity. The sample is N-type (dopant: Phosphorus) and un-oxidized. Effective lifetime is determined to be $\tau_{eff} = 87.7\ \mu s$ at an injection level of $\Delta n = 6.3x10^{15} cm^{-3}$.

6.3.1 Comparison with transmission

Figure 6.11 displays the data taken in both transmission mode and reflection mode of the intrinsic, un-passivated sample under the same conditions. The sample was tilted relative to the probe beam trajectory to allow the reflected part of the probe beam ($\lambda_{probe} = 1550\ nm$) to be monitored, while an identical detector was placed behind the sample allowing the transmitted part to be monitored as well. It is important to ensure that the same location of the sample is being measured in both reflection mode and transmission mode to avoid an erroneous comparison due to the spatial deviations in the lifetime of the sample. A pump wavelength of $\lambda_{pump} = 980\ nm$ is again selected to ensure that the light is absorbed uniformly throughout the depth of the sample.

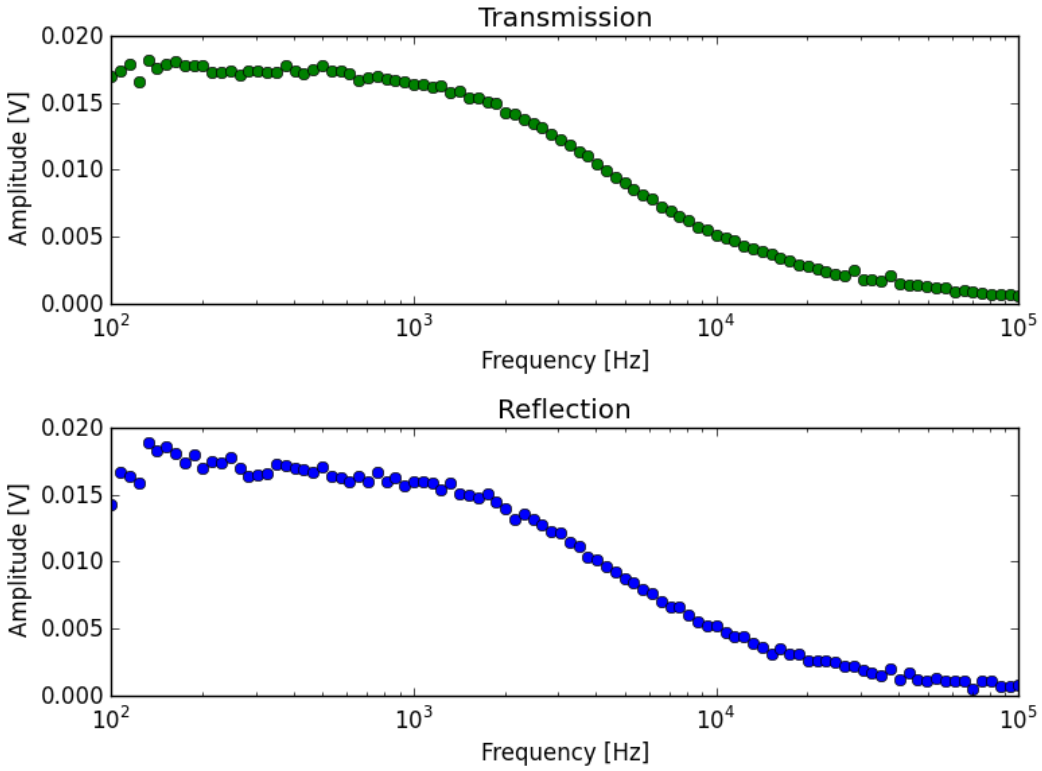

Figure 6.11: Transmission and Reflection mode roll off data measured on the same location of the intrinsic, un-passivated sample under equal injection levels.

The contour of the slope in the resulting Lorentzian roll off curves is uniquely determined by the effective lifetime of the sample measured. Therefore, if two roll off curves follow the same contour, one should expect that the same effective lifetime has been measured in either case. Such an overlap between the transmission and reflection mode data presented here is shown in figure 6.12.

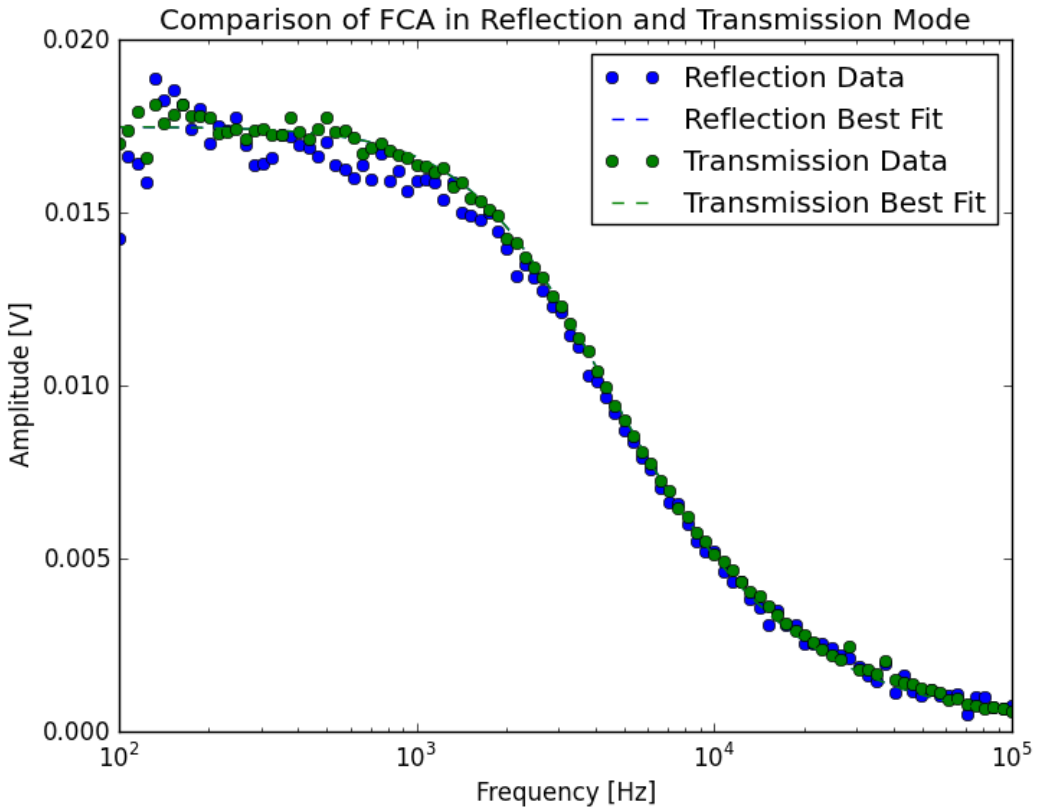

Figure 6.12: Overlap of Reflection mode and transmission mode data of the intrinsic and un-passivated sample. The calculated effective lifetimes are $\tau_{reflected} = 52.6\ \mu s$ and $\tau_{transmission} = 52.5\ \mu s$.

The overlap of the transmission mode and reflection mode frequency roll off curves is apparent in figure 6.12, however, a more convincing argument of their similarity is their calculated lifetimes as determined by fitting the curves to equation 5.1. Effective lifetimes of $\tau_{reflected} = 52.6\ \mu s$ and $\tau_{transmitted} = 52.6\ \mu s$ are calculated for the reflected and transmitted parts of the probe beam respectively.

6.3.2 Reflection Mode Data of Completed Solar Cell

We have shown that measurements made using the transmitted part and reflected part of the probe beam are equivalent. This allows us to confidently perform lifetime measurements on samples which do not allow for a transmission measurement, such as samples further along the production line which have a metalized back surface installed.

The measurements displayed in this section are performed in reflection mode on a completed solar cell. That is, a cell which has a textured front surface, metallized back surface, and metal fingers installed. The reflected light from the textured surface is very diffuse, and thus much less probe light will reach the detector. In order to increase the signal strength at the detector, a large area lens is placed between the sample and detector to capture scattered light and refocus it at the detector, as shown in figure 6.13.

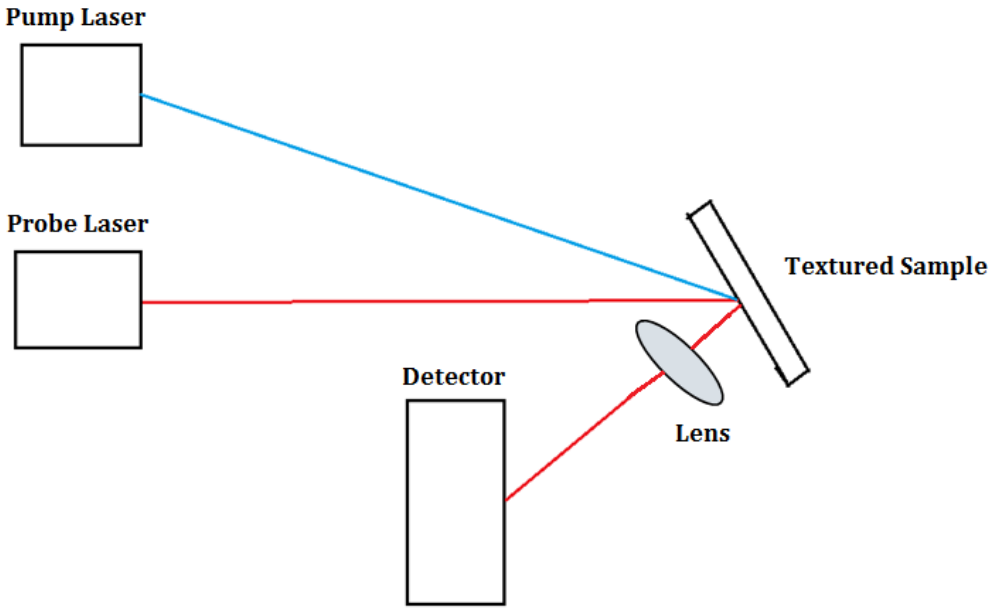

Figure 6.13: A lens is placed between a textured sample and the detector to capture diffuse reflection of the probe.

Though the placement of a lens between the sample and the detector allows for a greater percentage of probe light to be collected, the same is true of scattered light from the pump. Whereas the signal to pump ratio of polished wafers in transmission and

reflection mode was quite high (section 5.1), in the measurement of a textured sample this ratio is much lower, and the contribution from the pump cannot be ignored.

The pump wavelength has been decreased to $\lambda_{pump} = 808\ nm$ in order to increase the percentage of the pump beam that is absorbed, and minimize the intensity of the reflected part of the pump beam captured by the lens, and focused on the detector. An 808 nm notch filter has been placed over the aperture of the detector to further decrease the intensity of pump light detected. The probe laser wavelength remains $\lambda_{probe} = 1550\ nm$.

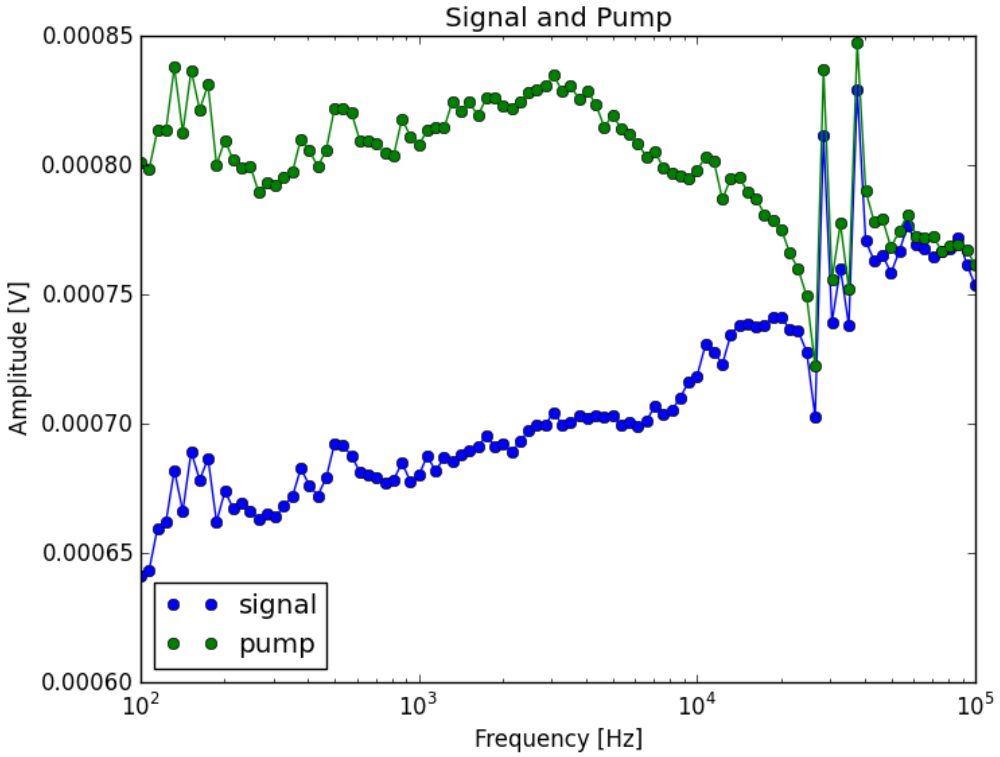

Figure 6.14: Reflection mode data of a textured, metallized, solar cell. The data presented in blue is of the experiment run with both the pump and probe beams at wavelengths of $\lambda_{pump} = 808nm$ and $\lambda_{probe} = 1550nm$ respectively. The data presented in green is collected when the experiment is run with only the pump beam.

Figure 6.14 displays two sets of data. The signal, shown in blue, is the output of the experiment when both the pump and probe lasers are incident on the sample. The pump, shown in green, is the output when only the pump laser is incident on the sample.

The lorentzian roll off is not seen in figure 6.14, however, there is a clear distinction between the data gathered from the experiment when run with both pump and probe as opposed to with the pump only.

It is important to note that the amplitude returned by the lock in amplifier and displayed in figure 6.14 is the magnitude of vector quantity, though the direction of the vector is not shown. As explained in section 5.1, in standard transmission and reflection mode measurements this is not an issue as the pump, probe, and background are sufficiently small that they may be ignored. The contribution of the pump may not be ignored in this case, as it is large compared with the pump-probe signal. By decomposing the data shown in figure 6.14 in to its vector components and subtracting the pump-probe data from the pump only data, the lorentzian roll off seen in figure 6.15 is produced. The effective lifetime is determined to be $\tau_{effective} = 13.8\ \mu s$, however, we note that an injection level is not included with the quoted lifetime for the solar cell. This is due to the inability to measure the total amount of light which has been absorbed in the material as a consequence of the textured surface as well as the metalized portions of the solar cell which may cause additional internal reflections in addition to shadowing from the metal fingers on the surface of the cell.

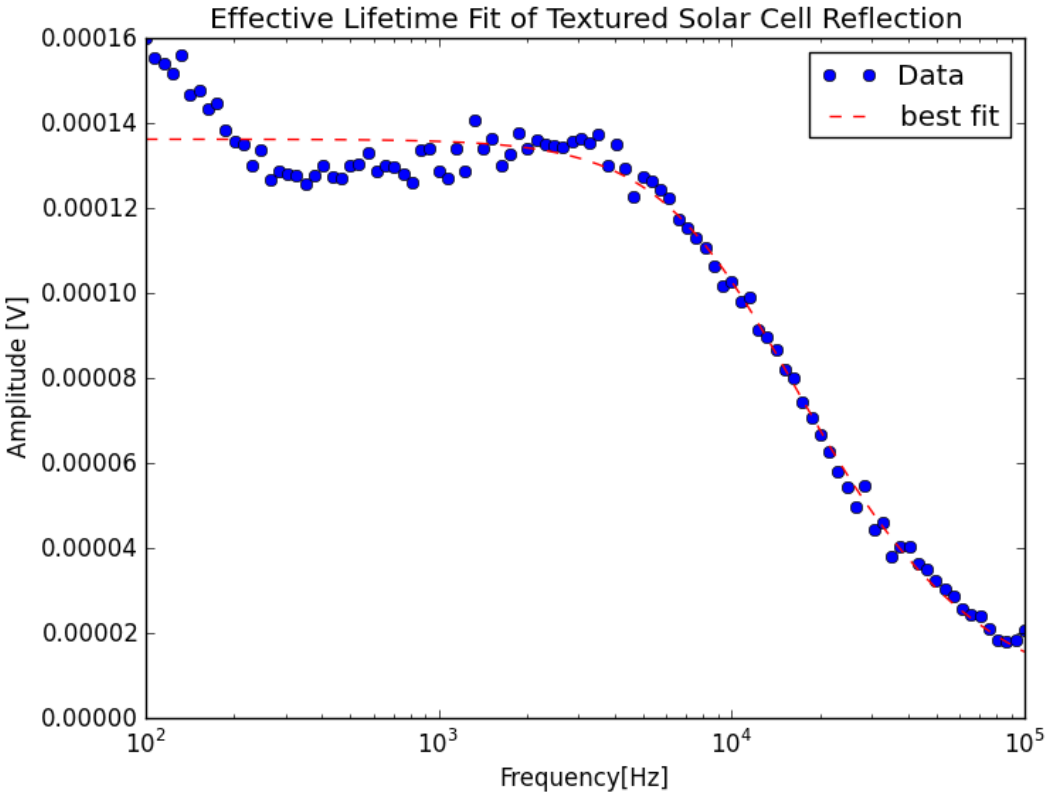

Figure 6.15: Lorentzian fit of reflection mode data gathered from a completed silicon solar cell. The effective lifetime is determined to be $\tau_{effective} = 13.8\ \mu s$.

7. Discussion

7.1 Injection Level Matching and Sample Uniformity

Lifetime maps of both the passivated and passivated intrinsic silicon samples as well as the 1.5mm N-type silicon sample have been performed with the Freiberg MW-PCD system and are displayed below in figures 7.1, 7.2, and 7.3 respectively.

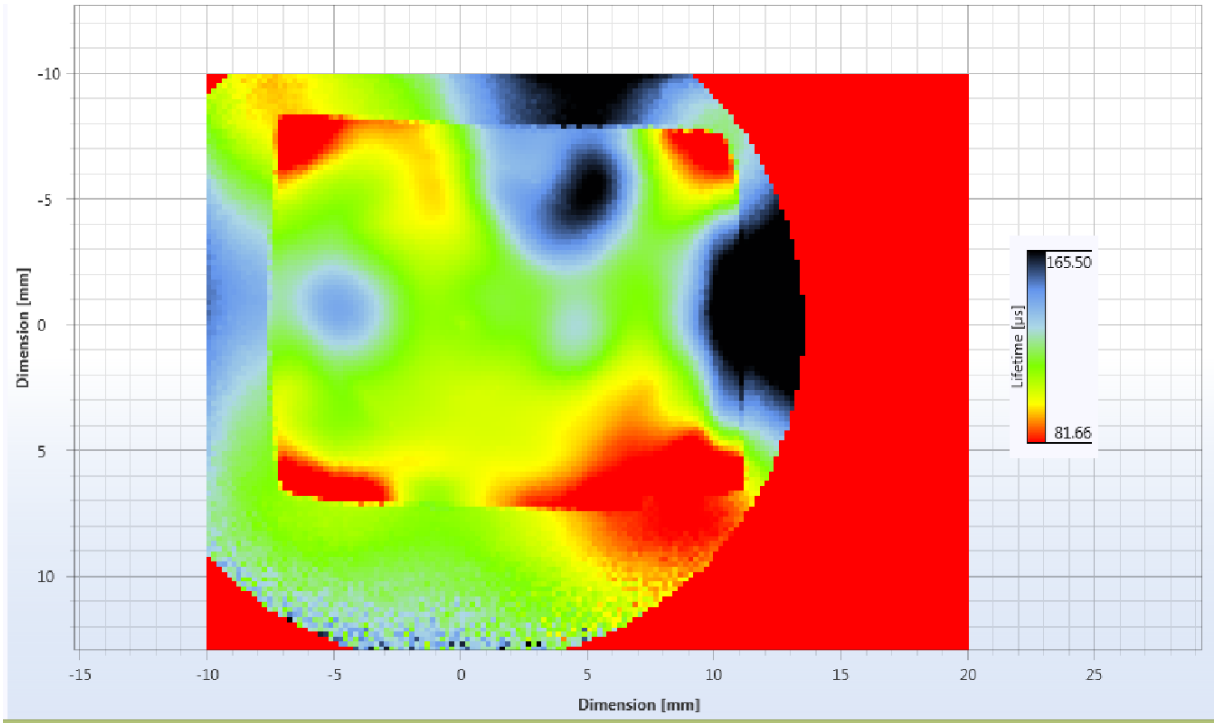

Figure 7.1: intrinsic, passivated silicon spatial lifetime map. Performed on the Freiberg MW-PCD system.

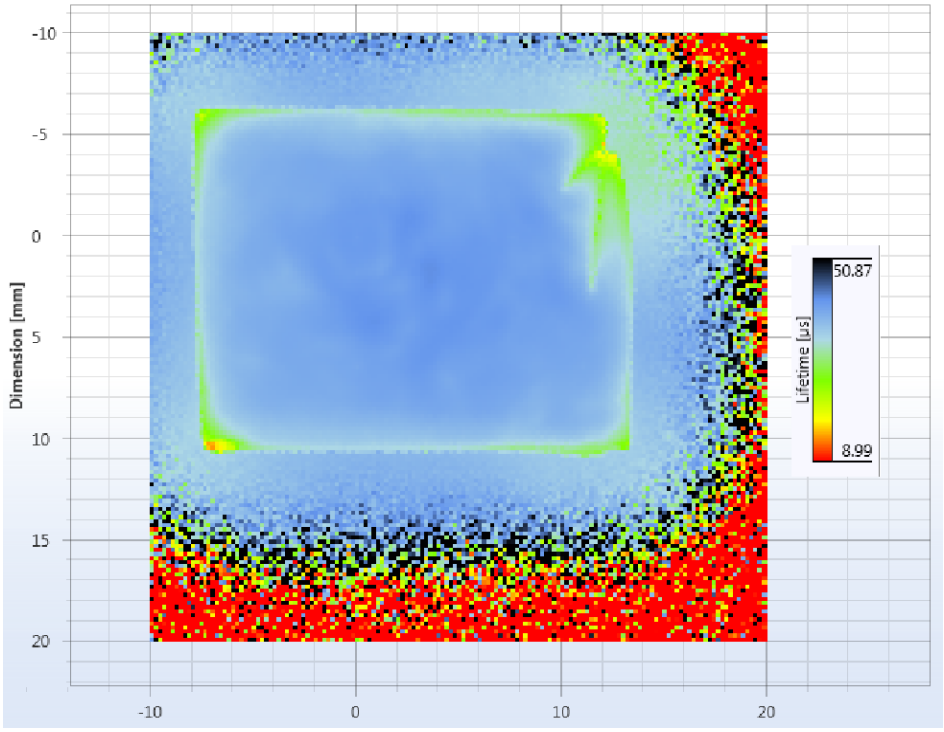

Figure 7.2: intrinsic, un-passivated silicon. Spatial lifetime map. Performed on the Freiberg MW-PCD system.

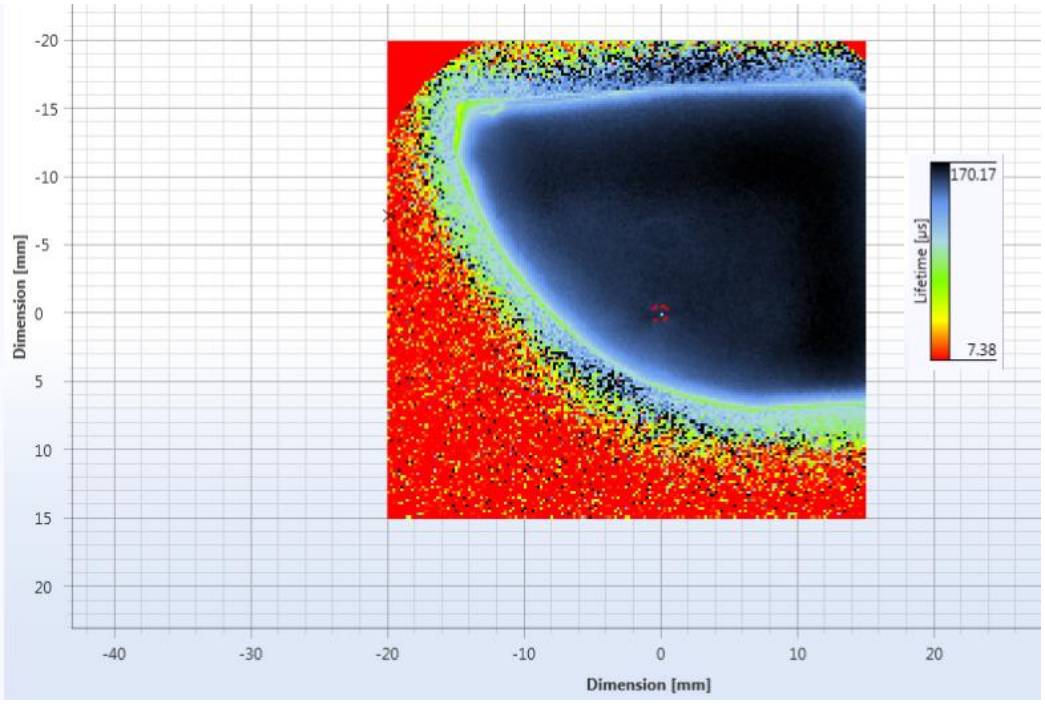

Figure 7.3: Lifetime map of the 1.5mm, N-type silicon sample. Performed on the Freiberg MW-PCD system.

The spatial variability in the lifetime of the passivated intrinsic silicon sample underscore the importance of ensuring that measurements are performed on the same location of the sample. It should be noted that although the deviation in lifetime across the un-passivated intrinsic sample and the 1.5 mm N-type sample are not as large as in the case of the passivated intrinsic sample, there is a degree of non-uniformity in the lifetime across the samples. This may have provided a source of error in injection level calculation, as expanding the area of the illuminated by the pump beam may cause two distinct lifetime regions of the sample to be measured simultaneously, leading to an erroneous calculation of effective lifetime.

7.2 repeatability

When considering the accuracy of this experiment's ability to measure effective lifetime, the repeatability of measurements must be accounted for. Figure 7.4 below shows the determined effective lifetime for twelve consecutive measurements. Those shown in red are measurements performed in reflection mode, and those shown in blue are performed in transmission mode – see section 6.3.1 concerning the equivalence of the two modes of measurement – on the same location of the sample.

A clear increase in measured lifetime is seen in successive runs of the experiment under the same conditions, with the average change in measured lifetime between runs being $\Delta\tau_{effective} = 0.955\ \mu s$. The mean lifetime measured over the twelve runs is $\tau_{mean} = 51.0\ \mu s$, and the maximum and minimum measured lifetimes are $\tau_{maximum} = 54.0\ \mu s$ and $\tau_{minimum} = 44.8\ \mu s$ repspectively. This gives a spread of $9.8\ \mu s$ between the lowest and highest measured lifetimes, or nearly 20% increase in measured lifetime when compared to the initial measurement.

Each iteration of the experiment requires fifteen minutes. As there is no known mechanism for lifetime to deviate this widely on such a timescale, an error in the measurement apparatus must be present. At this time, it is not known where in the experiment this error lies.

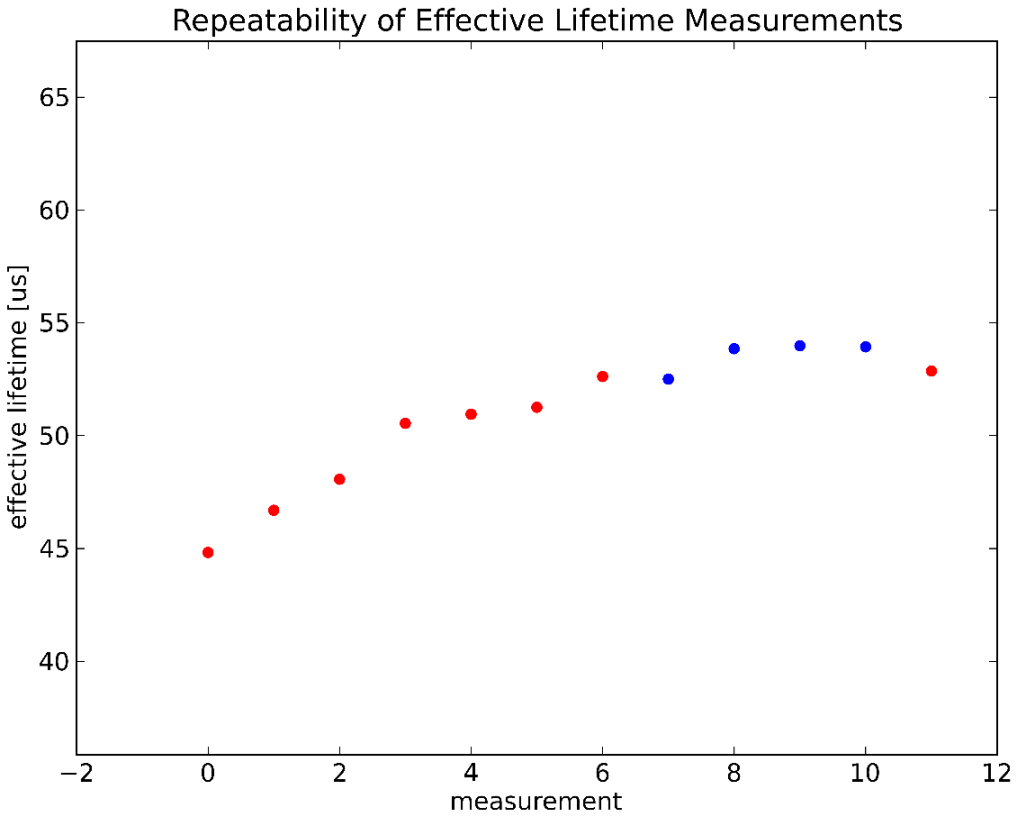

Figure 7.4: Repeatability measurements acquired on August 14 2017. All measurements are taken under identical conditions, and acquisition of a measurement begins immediately after the previous measurement has ended. Measurements shown in red are made in reflection mode and those shown in blue are made in transmission mode.

8. Conclusions

Pump-probe MFCA measurements of the effective minority carrier lifetime have been successfully demonstrated in transmission mode on intrinsic, float zone grown, silicon, both passivated and un-passivated, as well as on an N-type, un-passivated Czochralski grown silicon sample and a float zone grown N-type, un-passivated silicon sample. Reflection mode measurements have also been successfully demonstrated on the

Czochralski grown N-type as well as the un-passivated, intrinsic silicon sample. Using the latter sample, it has been shown that the effective minority carrier lifetime measured in transmission mode and reflection mode are equivalent, legitimizing the reflection mode measurement geometry.

Additionally, it has been shown that a signal is recoverable from the diffuse, scattered, reflection of the probe beam from a fully manufactured solar cell – complete with textured surface, metallized backing, and metal fingers. This has exciting consequences for semiconductor device manufacturing processes, in particular, solar cell fabrication. It is assumed that since MFCA measurements of effective lifetime may be performed on a bare silicon wafer, as well as a fully completed silicon solar cell, the technique must be effective at each processing step in between. Thus, it is possible for pump-probe MFCA measurements to be employed to monitor the effective lifetime of minority carriers at each processing step, allowing the manufacturer to determine at which stage the effective lifetime, and device efficiency, are degraded.

Some concerns over the accuracy of injection level determination remain, as well as the reliability of repeated measurements. A non-trivial trend of increasing values of measured effective lifetime can be seen for measurements performed in both transmission and reflection mode on the intrinsic, un-passivated sample. The same location of sample and injection level were used for each measurement, and from the spatial homogeneity of the lifetime of this sample it is reasonable to assume that even if the sample had shifted during measurement the measured effective lifetime should not change significantly.

In regards to the accuracy of injection level determination, the results are somewhat concerning. As the spatial uniformity of effective lifetime of the thick N-type sample is high, it can be reasonably assumed that expansion and contraction of the pump beam should not result in regions of differing effective lifetimes being measured simultaneously and thus does not explain the large discrepancy in effective lifetime between measurements of similar injection levels. Small deviations in the placement of the lens, such as distance from the sample or angle relative to the sample will alter the area of the sample which is illuminated by the pump beam. As the magnification of the

lens becomes greater to increase the injection level, and the area of the pump beam decreases, small deviations in lens placement become a greater source of error. It is possible that vibrations present in the laboratory during measurement may have shifted the position of the lens, and these errors may be decreased in the future by floating the bench, however, deviations in the area illuminated by the pump are not sufficient on their own to explain the large deviations from the expected injection level dependence of the effective lifetime. Both the injection level dependence as well as repeatability of measurement of the pump-probe MFCA method require further study, however, the work presented here shows MFCA to be a promising technique for non-contact monitoring of minority carrier lifetime.

Works Cited

[1] V Grivickas, "Carrier Lifetime: Free Carrier Absorption, Photoconductivity, and Photoluminescence," *Charact. Mater.*, 2002.

[2] P. Würfel and U. Würfel, *Physics of Solar Cells: From Basic Principles to Advanced Concepts*, 3rd edition. Weinheim: Wiley-VCH Verlag GmbH & Co. KGaA, 2016.

[3] http://www.pveducation.org/pvcdrom/solar-cell-structure

[4] S. Rein, *Lifetime Spectroscopy: a Method of Defect Characterization in silicon for photovoltaic applications ; with 29 tables*. Berlin: Springer, 2005.

[5] P. F. Baude, T. Tamagawa, and D. L. Polla, "Contactless Optical Evaluation of Processing Effects on Carrier Lifetime in Silicon," *Appl. Phys. Lett.*, vol. 57, no. 24, pp. 2579–2581, Dec. 1990.

[6] M. De Laurentis and A. Irace, "Optical Measurement Techniques of Recombination Lifetime Based on the Free Carriers Absorption Effect," *J. Solid State Phys.*, vol. 2014, pp. 1–19, 2014.

[7] S. M. Sze and K. K. Ng, *Physics of Semiconductor Devices*, 3rd ed. Hoboken, N.J: Wiley-Interscience, 2007.

[8] J. Linnros, "Carrier Lifetime Measurements Using Free Carrier Absorption Transients. I. Principle and Injection Dependence," *J. Appl. Phys.*, vol. 84, no. 1, pp. 275–283, Jul. 1998.

[9] A. Cuevas and D. Macdonald, "Measuring and Interpreting the Lifetime of Silicon Wafers," *Sol. Energy*, vol. 76, no. 1–3, pp. 255–262, Jan. 2004.

[10] K. Watanabe, "Increase in Effective Carrier Lifetime of Silicon at Low Carrier Injection Levels," *Semicond. Sci. Technol.*, vol. 9, no. 4, p. 370, 1994.

[11] B. Berger, N. Schüler, S. Anger, B. Gründig-Wendrock, J. R. Niklas, and K. Dornich, "Contactless Electrical Defect Characterization in Semiconductors by Microwave Detected Photo Induced Current Transient Spectroscopy (MD-PICTS) and Microwave Detected Photoconductivity (MDP)," *Phys. Status Solidi A*, vol. 208, no. 4, pp. 769–776, Apr. 2011.

[12] R. A. Sinton and A. Cuevas, "Contactless Determination of Current–Voltage Characteristics and Minority-Carrier Lifetimes in Semiconductors from Quasi-Steady-State Photoconductance Data," *Appl. Phys. Lett.*, vol. 69, no. 17, pp. 2510–2512, Oct. 1996.

[13] M. J. Kerr, A. Cuevas, and R. A. Sinton, "Generalized Analysis of Quasi-Steady-State and Transient Decay Open Circuit Voltage Measurements," *J. Appl. Phys.*, vol. 91, no. 1, p. 399, 2002.

[14] H. Nagel, C. Berge, and A. G. Aberle, "Generalized Analysis of Quasi-Steady-State and Quasi-Transient Measurements of Carrier Lifetimes in Semiconductors," *J. Appl. Phys.*, vol. 86, no. 11, pp. 6218–6221, Dec. 1999.

[15] M. Schöfthaler and R. Brendel, "Sensitivity and Transient Response of Microwave Reflection Measurements," *J. Appl. Phys.*, vol. 77, no. 7, pp. 3162–3173, Apr. 1995.

[16] A. G. Aberle, J. Schmidt, and R. Brendel, "On the Data Analysis of Light-Biased Photoconductance Decay Measurements," *J. Appl. Phys.*, vol. 79, no. 3, pp. 1491–1496, Feb. 1996.

[17] N. J. Harrick, "Lifetime Measurements of Excess Carriers in Semiconductors," *J. Appl. Phys.*, vol. 27, no. 12, pp. 1439–1442, Dec. 1956.

[18] D. K. Schroder, R. N. Thomas, and J. C. Swartz, "Free Carrier Absorption in Silicon," *IEEE J. Solid-State Circuits*, vol. 13, no. 1, pp. 180–187, 1978.

[19] D. E. Houston, S. Krishna, and E. D. Wolley, "Study of Charge Dynamics in High Speed Power Devices Using Free Carrier Absorption Measurements," in *Electron Devices Meeting, 1976 International*, 1976, pp. 504–507.

[20] Sanii, F., R. J. Schwartz, R. F. Pierret, and W. M. Au. "The Measurement of Bulk and Surface Recombination by Means of Modulated Free Carrier Absorption." In *Photovoltaic Specialists Conference, 1988., Conference Record of the Twentieth IEEE*, pp. 575-580. IEEE, 1988.

[21] V. Grivickas, J. Linnros, A. Vigelis, J. Šečkus, and J. A. Tellefsen, "A Study of Carrier Lifetime in Silicon by Laser-Induced Absorption: A Perpendicular Geometry Measurement," *Solid-State Electron.*, vol. 35, no. 3, pp. 299–310, 1992.